DRUG DEVELOPMENT

An orally active, small-molecule TNF inhibitor that disrupts the homotrimerization interface improves inflammatory arthritis in mice

Nasir Javaid[1]†, Mahesh Chandra Patra[1]†, Da-Eun Cho[2]†, Maria Batool[1,3], Yoongeun Kim[2], Gwang Muk Choi[2], Moon Suk Kim[1], Dae-Hyun Hahm[2,4]*, Sangdun Choi[1,3]*

Excessive signaling by the proinflammatory cytokine TNF is involved in several autoimmune diseases, including rheumatoid arthritis (RA). However, unlike the approved biologics currently used to treat this and other conditions, commercially available small-molecule inhibitors of TNF trimerization are cytotoxic or exhibit low potency. Here, we report a TNF-inhibitory molecule (TIM) that reduced TNF signaling in vitro and was an effective treatment in a mouse model of RA. The initial lead compound, TIM1, attenuated TNF-induced apoptosis of human and mouse cells by delaying the induction of proinflammatory NF-κB and MAPK signaling and caspase 3– and caspase 8–dependent apoptosis. TIM1 inhibited the secretion of the proinflammatory cytokines IL-6 and IL-8 by disrupting TNF homotrimerization, thereby preventing its association with the TNF receptor. In a mouse model of collagen-induced polyarthritis, the more potent TIM1 analog TIM1c was orally bioavailable and reduced paw swelling, histological indicators of knee joint pathology, inflammatory infiltration of the joint, and the overall arthritis index. Orally delivered TIM1c showed immunological effects similar to those elicited by intraperitoneal injection of the FDA-approved TNF receptor decoy etanercept. Thus, TIM1c is a promising lead compound for the development of small-molecule therapies for the treatment of RA and other TNF-dependent systemic inflammation disorders.

INTRODUCTION

The tumor necrosis factor (TNF) superfamily constitutes a group of pleiotropic proinflammatory cytokines that are essential for several important physiological processes, such as host protection against pathogens and tumors (*1*, *2*). Dysregulated signaling by TNF superfamily members (particularly TNF itself) is implicated in several pathological conditions, including rheumatoid arthritis (RA), psoriasis (*3*), and inflammatory bowel disease (*4*). Chronic overproduction of TNF is also associated with Alzheimer's disease (*5*), major depression (*6*), and cancer (*7*). Thus, substantial efforts have been made to disrupt TNF signaling pathways using a variety of therapeutic modulators (*8*).

TNF is initially synthesized as a 26-kDa, 233–amino acid transmembrane protein that is released by proteolytic cleavage (by TNF-α–converting enzyme) as a 17-kDa, 157–amino acid soluble protein. The soluble TNF spontaneously assembles itself into a stable homotrimer, which is the biologically active form of this cytokine (*9*). TNF is mainly produced by macrophages, T lymphocytes, and natural killer cells and is recognized by two distinct receptors, TNF receptor 1 (TNFR1) and TNFR2, eliciting different downstream signaling events (*10*, *11*). Although TNFR1 is ubiquitously produced by all cell types, the production of TNFR2 is limited to immune cells; therefore, the binding of TNF to either receptor results in diverse functional consequences (*12*, *13*). The downstream signaling pathway of TNFR1 and TNFR2 typically activates the transcription factor nuclear factor κ light chain enhancer of activated B cells (NF-κB) and members of mitogen-activated protein kinase (MAPK) signaling cascades, such as extracellular signal–regulated kinase (ERK), p38, and c-Jun N-terminal kinase (JNK) (*14*). It also activates various caspases that participate in the process of apoptosis (*15*). The activation of NF-κB and MAPKs plays an important role in the induction of proinflammatory cytokines and immunoregulators, mounting a strong inflammatory response that often results in the apoptosis or necrosis of most cell types (*16*). The activation of TNFR2 also participates in the development of cancer, which makes it a potential target for antitumor immunotherapy (*17*, *18*).

Early evidence suggested that dysregulation of TNF production is associated with chronic arthritis in mouse models and that the application of TNF inhibitors is effective against the disease (*19*). This observation aroused much interest among anti-TNF manufacturers, leading to the first successful clinical trials in RA (*20*) and other chronic inflammatory diseases, such as Crohn's disease, psoriasis, psoriatic arthritis, juvenile idiopathic arthritis, spondyloarthritis, and Behçet's disease (*21*). The drugs currently approved for the treatment of inflammatory diseases are synthetic monoclonal antibodies, such as infliximab, adalimumab, certolizumab, and golimumab, or soluble receptor fusion proteins such as etanercept (ETN); all these biological therapeutics bind to soluble TNF and prevent its association with cell surface TNFR1 or TNFR2 (*22*). Although these biologics are successful in the clinic, they are highly expensive, not orally bioavailable, and often undermine the host immunity against latent or recurring infections (*23*). Moreover, the high–molecular weight biologics cannot be applicable to the central nervous system diseases associated with high TNF signaling, such as Alzheimer's disease. Several small-molecule compounds

[1]Department of Molecular Science and Technology, Ajou University, Suwon 16499, Korea. [2]Department of Biomedical Sciences, Graduate School, Kyung Hee University, Seoul 02447, Korea. [3]S&K Therapeutics, Ajou University Campus Plaza 418, 199 Worldcup-ro, Yeongtong-gu, Suwon 16502, Korea. [4]Department of Physiology, College of Medicine, Kyung Hee University, Seoul 02447, Korea.
*Corresponding author. Email: dhhahm@khu.ac.kr (D.-H.H.), sangdunchoi@ajou.ac.kr (S.C.)
†These authors contributed equally to this work.

have been successful in preclinical studies, demonstrating prospects for future clinical applications (*24*–*28*). Therefore, small-molecule–based therapies are considered potential alternatives to TNF inhibition by biologics (*29*). The crystal structure of the first small-molecule antagonist of TNF, SPD304, which has an equilibrium dissociation constant (K_D) value of 5.36 μM and disrupts TNF trimerization (*24*), has enabled researchers to develop other small-molecule ligands through structure-based drug design. A subsequent study revealed the structure of TNF bound to multiple molecules of the compound JNJ525, indicating possible aggregation-mediated TNF inhibition (*25*). Studies also uncovered small-molecule agents that directly bind to TNF with half-maximal inhibitory concentrations (IC_{50}) ranging from 1 to 50 μM and block the TNFR1- or TNFR2-mediated downstream signaling pathways (*30*–*36*). Several natural product–like compounds have also been found to inhibit TNF-mediated cellular effects in both in vitro and in vivo studies (*32*, *37*, *38*). Despite the preclinical advancement of the anti-TNF small-molecule candidate therapeutics, the low potency and high toxicity of these chemical agents have limited their testing in clinical trials.

In the present study, our purpose was to identify a small-molecule TNF inhibitor through a combined structure-based and ligand-based virtual screening approach. The in vitro bioassays revealed that the starting lead compound, TNF-inhibitory molecule 1 (TIM1), prominently inhibited TNF-induced secretion of cytokines by human cell lines and attenuated TNF-induced death in both human and mouse cells without any cytotoxicity up to a concentration of 200 μM. A cross-linking protein interaction analysis followed by surface plasmon resonance (SPR) spectroscopy and computational modeling suggested that TIM1 could stably occupy the central hydrophobic pocket in the TNF homodimer and prevent the formation of a functional homotrimer. One of the potent TIM1 derivatives, TIM1c, showed oral bioactivity in a mouse model of collagen-induced polyarthritis (CIA) and suppressed arthritis symptoms. We envision that the TIM series of ligands will be valuable for the development of low–molecular weight therapeutic agents targeting TNF-mediated inflammatory diseases.

RESULTS

Identification of TIM1 as an inhibitor of TNF

The identification of a new TNF inhibitor, TIM1, was carried out by an in silico approach using the crystal structure of the TNF-SPD304 complex [Protein Data Bank (PDB) ID: 2AZ5] and a multiconformational chemical compound library obtained from various sources (Table 1). The compounds having drug-like physiochemical properties were isolated by means of a fingerprint-based Tanimoto coefficient similarity metric using the selected TNF inhibitors in the query (Table 2 and Fig. 1A). The resultant ligand library was then screened through pharmacophore models of SPD304 and JNJ525 ligands (Fig. 1, B and C), which have well-defined intermolecular interactions with TNF (*24*, *25*). The resulting set of 15,668 ligands was then subjected to structure-based virtual screening in the central hydrophobic cavity of the TNF homodimer. The ligand poses were ranked by the Merck molecular force field 94x (MMFF94x)–based binding free energy (GBVI/WSA ΔG) scores. In silico toxicity analysis was performed on the top-scoring 100 ligands through both online and offline computational tools, including the removal of pan-assay interference compounds (PAINS). The top 10 ligands without any predicted toxic fragments in their chemical structures were procured for the in vitro validation of their bioactivity.

The 10 purchased chemical compounds (TIM1 to TIM10) were initially tested for toxicity in human dermal fibroblasts (HDFs) at concentrations ranging from 1 to 50 μM. Cell viability was monitored by the colorimetric 3-(4,5-dimethylthiazol-2-yl)-2,5-diphenyl-2*H*-tetrazolium bromide (MTT) assay after 24 hours of treatment with each compound. Of the tested molecules, TIM1 (Fig. 1D) showed no cytotoxicity, whereas the other compounds were cytotoxic (Fig. 2A). The toxicity data were used to predict the median lethal concentration (LC_{50}) value of TIM1 to TIM10 by ATT Bioquest LC_{50} calculator (table S1). It is noteworthy that the positive controls, SPD304 and C87, manifested cytotoxicity in our experiments at or below 50 μM (Fig. 2A). TIM1 caused no cell death in HDFs (fig. S1A) or murine fibrosarcoma L929 cells (fig. S1B) up to 200 μM. On the basis of the observed cytotoxicity of the compounds, TIM1 was chosen for further experiments to examine its inhibitory effect on the TNF-induced secretion of cytokines. A preincubated mixture of recombinant human TNF (rhTNF) with either TIM1 or SPD304 was applied to HDFs, and the culture supernatant was collected after 24 hours for evaluation of the cytokine secretion profile by enzyme-linked immunosorbent assays (ELISAs). TIM1 inhibited the TNF-induced secretion of interleukin-8 (IL-8; Fig. 2B) and IL-6 (Fig. 2C) in a concentration-dependent manner. The IC_{50} of TIM1 against IL-8 and IL-6 secretion was found to be 17.5 and 20.37 μM, respectively (Fig. 2, D and E). Although SPD304 inhibited the secretion of IL-8 or IL-6 completely at 25 μM, this remarkable inhibition was due to its severe cytotoxicity at concentrations greater than 10 μM (Fig. 2F). At 10 μM, however, SPD304 increased the secretion of the cytokines (Fig. 2, B and C). This variable cellular behavior was most probably due to the physiological stress experienced by the cells before necroptosis due to the toxic effects of the drug (*39*). We observed the death of HDFs at 10 μM SPD304 (Fig. 2A); however, it was not the case on cotreating SPD304 with TNF (Fig. 2F). This variable response was likely due to the activation of prosurvival and proliferative signaling pathways through TNFR1 and TNFR2 (*40*, *41*). The death of HDFs at higher concentrations of SPD304 (25 to 100 μM) in the presence of TNF (1 ng/ml) indicates that the survival of HDFs probably depends on the relative amounts of SPD304 and TNF in the assay (Fig. 2F).

TIM1 prevents the TNF-induced apoptosis of human and mouse cells

TNF is a potent inducer of cell death through the activation of TNFR1-associated death signaling pathways (*42*). To assess the preventive effect of TIM1 on TNF-induced cell death, we applied different concentrations of TIM1 or SPD304 (preincubated with rhTNF) to actinomycin D (act-D)–sensitized HDFs. A marked attenuation of the TNF-induced death was observed upon treatment with TIM1 (Fig. 3, A and B), whereas such an effect was not exerted by SPD304 at concentrations higher than 1 μM (Fig. 3, A and B). To test whether TIM1 exerted a protective effect on mouse cells, we applied the preincubated mixtures of either TIM1 or SPD304 and recombinant mouse TNF (rmTNF) to the act-D–sensitized L929 cell line. According to expectation, TIM1 inhibited the rmTNF-induced death pathway in L929 cells in a concentration-dependent manner (Fig. 3, C and D). On the other hand, SPD304 failed to attenuate the death of these cells at concentrations other than 1 μM

Table 1. Chemical compound libraries used for the screening of TNF inhibitors. The ligands were obtained from the ZINC database (https://zinc.docking.org/).

Compound library	No. of compounds
Zinc drug-like	14,480,911
Zinc lead-like	5,449,805
Enamine	3,005,135
ChemBridge	1,586,299
ChemDiv	1,912,842
Life Chemicals	497,067
Maybridge	70,780
Total	27,002,839

Table 2. Ligands used to screen the compound library through molecular fingerprints.

Inhibitor name	Target	Activity	Reference
SPD304	TNF	IC_{50} = 22 μM	(*24*)
Physcion-8-*O*-β-D-monoglucoside	TNFR1	K_D = 376 nM	(*37*)
JNJ525	TNF	$IC_{50} \asymp$ 1.2 μM	(*25*)
AP-906/41640035	TNF	IC_{50} = 14 μM	(*33*)
Quinuclidine 1	TNF/TNFR1 interface	$IC_{50} \asymp$ 5 μM	(*47*)
Indoloquinolizidine 2	TNF/TNFR1 interface	$IC_{50} \asymp$ 10 μM	(*47*)
Japonicone A	TNF/TNFR1 interface	$IC_{50} \asymp$ 10 μM	(*38*)
Inhibitor 1	TNF	IC_{50} = 10 μM	(*35*)
C87	TNF	IC_{50} = 8.73 μM	(*34*)
Erythrosine B	TNF/TNFR1 interface	IC_{50} = 5 μM	(*65*)

(Fig. 3, C and D). TNF-induced apoptosis is histologically characterized by nuclear fragmentation, nuclear and cytoplasmic condensation, and persistence of membrane integrity (black arrows in Fig. 3, B and D). TIM1 reversed the development of these morphological changes in HDFs and L929 in a concentration-dependent manner (white arrows in Fig. 3, B and D).

TIM1 suppresses multiple TNF-dependent signaling pathways

The activation of TNFR1 by TNF triggers several distinct signaling pathways, including NF-κB, MAPK, and caspase pathways (*43*). We first evaluated the effect of TIM1 at 20 μM concentration (near IC_{50} value) on the phosphorylation of the p65 subunit, which is an essential indicator of NF-κB activation, in L929 cells by Western blotting (Fig. 4A and fig. S2). TNF-induced phosphorylation of p65 was significantly attenuated by TIM1, unlike untreated cells in which the amount of phosphorylated p65 increased over time. TNF-induced phosphorylation of the MAPKs p38, JNK, and ERK was also significantly inhibited by TIM1 (Fig. 4A and fig. S2). Furthermore, TIM1 inhibited the TNF-induced activation of caspases that is a hallmark of programmed cell death. Specifically, TNF-induced formation of cleaved, activated forms of caspase 8 (c-Cas8) and caspase 3 (c-Cas3) peaked at 5 hours and 8 to 12 hours, respectively, and this was significantly attenuated by TIM1 (Fig. 4B and fig. S3).

TIM1 and its derivatives potently inhibit TNF-induced cell death and cytokine secretion

To improve the TNF-inhibitory activity of TIM1, we conducted additional experiments with two subsets of commercially available (60 to 80% similar) derivatives and compared their activities with those of TIM1 and SPD304. The cytotoxicities of these derivatives, sorted into two subsets (TIM1a to TIM1o and TIM1-1 to TIM1-12), were determined by MTT assay on L929 cells (figs. S4A and S5A) and HDFs (figs. S4B and S5B). Among the first subset, TIM1c, TIM1d, and TIM1i showed negligible toxicity and a comparatively better suppression of TNF-induced cell death than others on L929 cells (fig. S6) and HDFs (fig. S7). Among the second subset, TIM1-9 and TIM1-12 showed negligible toxicity on L929 (fig. S5A) and HDFs (fig. S5B). Subsequently, preincubated mixtures of rhTNF with TIM1, its selected derivatives, or SPD304 were applied to HDFs, and the culture supernatants were evaluated by ELISA for the magnitude of IL-8 and IL-6 secretion. Of the tested molecules, TIM1c, TIM1d, TIM1-9, and TIM1-12 (fig. S8) manifested negligible cytotoxicity and greater inhibition of TNF-driven induction of IL-8 and IL-6 in comparison with TIM1i in a concentration-dependent manner (Fig. 5A). The tested molecules also suppressed TNF-induced cell death of HDFs and L929 cells in a concentration-dependent manner (Fig. 5B). In particular, TIM1c caused the strongest inhibition of the TNF-driven induction of IL-8 and IL-6 and cell death and was assumed to be the most potent derivative. It should be noted here that, although SPD304 completely inhibited IL-8 and IL-6 production at 50 μM, this compound is extremely cytotoxic above 1 μM (Fig. 2A), rendering the observed cytokine inhibition irrelevant.

TIM1 and TIM1c prevent homotrimerization of TNF by directly binding to the TNF monomer

After confirming the inhibition of the TNF signaling pathway by TIM1 and TIM1c, we sought to verify their mechanism of action in a cross-linking protein interaction assay followed by Western blot analyses. TNF is biologically active in solution in the form of a stable homotrimer, and ligands that interfere with the trimeric assembly are known to inactivate the cytokine function (*24*, *25*, *32*). Because the initial screening of ligands was carried out by considering the small-molecule–binding site of the TNF three-dimensional structure, we anticipated that TIM1 and TIM1c would block TNF activity by inhibiting the formation of the functional trimer. To test this hypothesis, TNF was preincubated with TIM1, TIM1c, or SPD304; chemically cross-linked; and then analyzed by Western blotting. As expected, all three molecules attenuated the formation of functional homotrimers by both rhTNF (Fig. 5C and fig. S9) and rmTNF (Fig. 5D and fig. S10) in a concentration-dependent manner as compared with nontreated cross-linked control. Further, to confirm whether TIM1 and its most potent derivative, TIM1c, could directly bind to TNF, we carried out an SPR

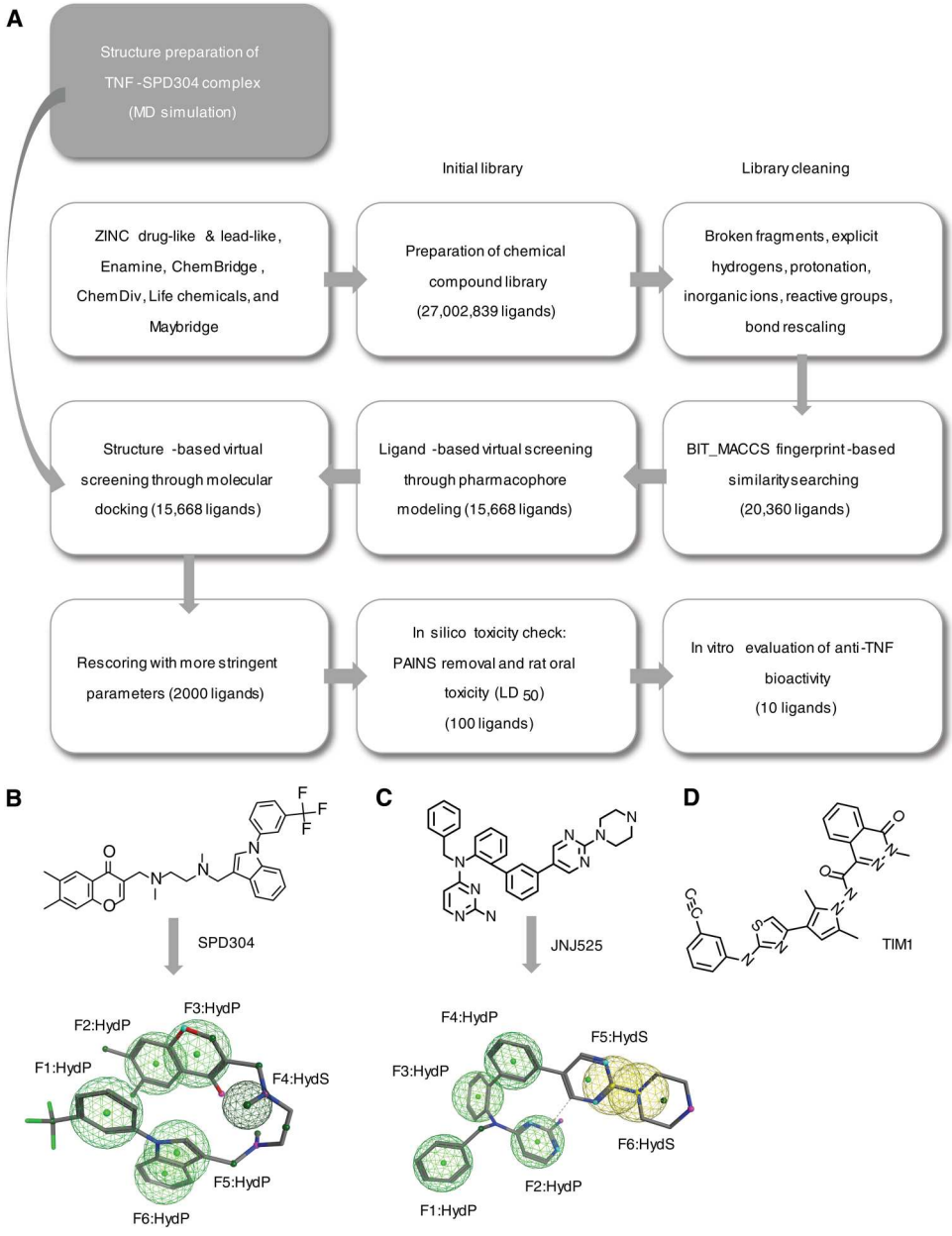

Fig. 1. Workflow of the virtual screen. (**A**) Schematic representation of chemical library preparation and virtual screening. The number of compounds included in each stage of the screen is indicated in parentheses. (**B** to **D**) Two-dimensional structures of the known TNF inhibitors, SPD304 (PDB ID: 2AZ5) (B) and JNJ525 (PDB ID: 5MU8), (C) and the active compound we identified, TIM1 (D). The pharmacophore models of SPD304 and JNJ525 used for the ligand-based virtual screening are also shown. LD_{50}, median lethal dose.>

spectroscopy experiment by immobilizing TNF on the sensor chip. The SPR sensogram showed that TIM1 and TIM1c bound to immobilized rmTNF and rhTNF in a concentration-dependent manner (Fig. 6, A to D). The K_D values for TIM1 with rmTNF, TIM1 with rhTNF, TIM1c with rmTNF, and TIM1c with rhTNF were calculated as 1.55 ± 0.32 μM (Fig. 6A), 0.68 ± 0.26 μM (Fig. 6B), 94.6 ± 4.4 μM (Fig. 6C), and 1183 ± 110 μM (Fig. 6D), respectively. These findings indicated that TIM1 and TIM1c likely bind to the central hydrophobic cavity of the TNF monomer, thereby preventing the formation of the functional homotrimer.

Molecular dynamics predicts that TIM1 and TIM1c stably occupy the TNF homodimer through nonpolar interactions

We performed molecular dynamics (MD) simulations of complexes hTNF-SPD304, hTNF-TIM1, and hTNF-TIM1c for 100 ns each to compare the ligand-binding patterns under dynamic conditions (fig. S11). The simulations showed TIM1 binding to the TNF dimer in a more extended conformation than SPD304 (Fig. 6E), with the thiazole ring packed against Tyr^{119} in chain A and Tyr^{119*} in chain B and the carboxamide-linked pyrrole group interacting mainly with Gln^{61} and Tyr^{151} in chain A (Fig. 6F). The

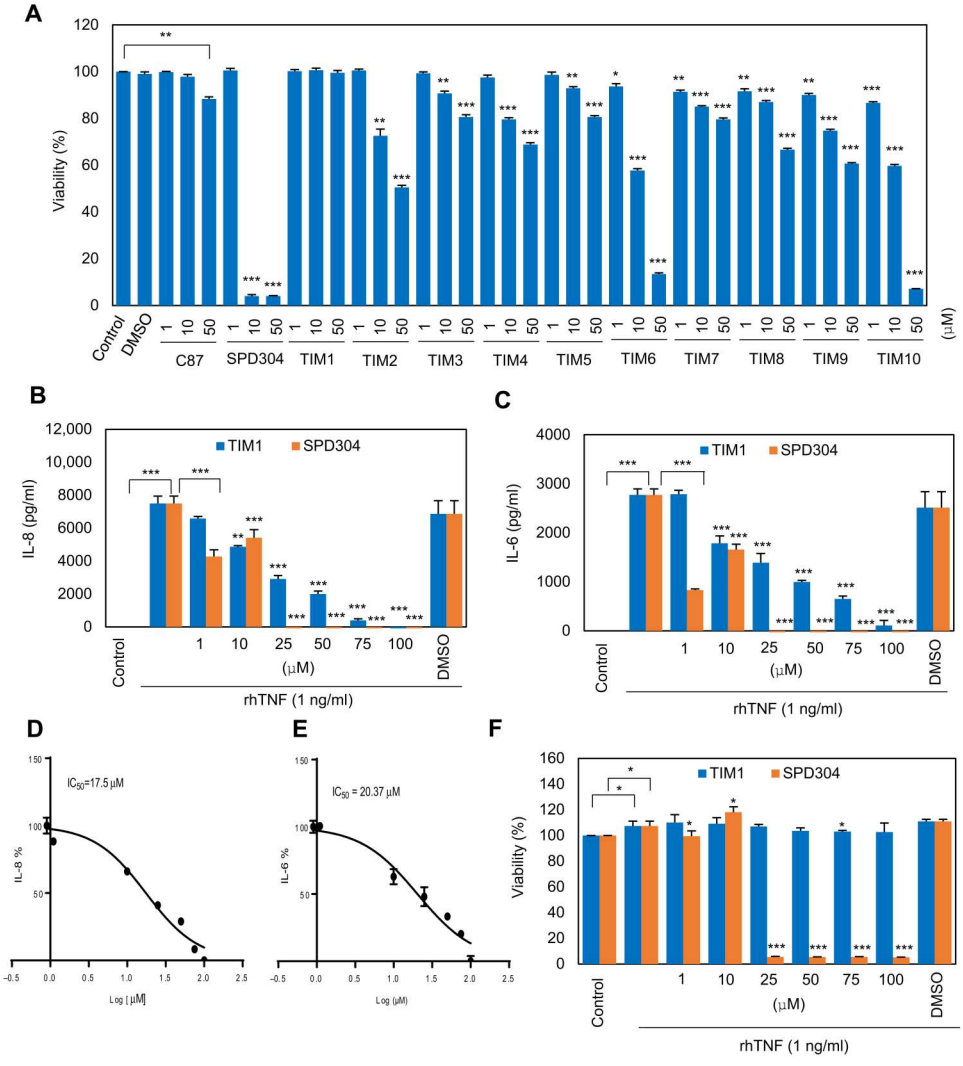

Fig. 2. Screening and identification of potential TNF inhibitors. (**A**) Cell viability analysis (MTT assay) of human dermal fibroblasts (HDFs) treated for 24 hours with the indicated concentrations of the 10 in silico–derived TNF inhibitor candidates. The TNF inhibitors C87 and SPD304 were positive controls. $n = 3$ independent experiments. (**B** and **C**) Quantification of IL-8 (B) and IL-6 (C) secreted by HDFs that were stimulated for 24 hours with rhTNF that had been preincubated with the indicated concentration of TIM1 or SPD304 for 1 hour. The data were normalized to unstimulated control cells. $n = 4$ independent experiments. (**D** and **E**) IC_{50} curves for TIM1 inhibition of IL-8 (D) and IL-6 (E) secretion by HDFs. $n = 4$ independent experiments. (**F**) Cell viability analysis of HDFs stimulated with rhTNF preincubated with the indicated concentration of TIM1 or SPD304. $n = 4$ independent experiments. All quantitative data represent means ± SEM of three or more independent experiments and evaluated by two-tailed paired Student's t test (*$P < 0.05$, **$P < 0.01$, and ***$P < 0.001$).

phthalazine group was stabilized by a partial π-stacking interaction with Tyr^{59} and hydrophobic contacts with Tyr^{151} and His^{15}. The ethynylphenyl group interacted with Val^{123}, Leu^{57}, and Ile^{155} and Tyr^{151*}, Tyr^{59*}, and Ile^{155*}. TIM1 did not form any salt bridges or hydrogen bonds with TNF, except for a single electrostatic interaction between the amide nitrogen of TIM1 and the hydroxyl group of the Tyr^{151} side chain. The oxygen atoms of the ligand were exposed to the solvent, whereas the electronegative atoms of SPD304 (such as the 3-trifluoromethyl moiety) interacted with the TNF hydrophobic core.

TIM1c, on the other hand, was modeled to bind to the TNF homodimer in a completely extended but partially planar orientation (Fig. 6G). In TIM1c, the ethynylphenyl group is substituted with the propylamine group, which stretched toward a hydrophobic pocket formed by Ala^{96*}, Pro^{117*}, Ile^{118*}, and Leu^{120*}. In contrast to TIM1, the thiazole ring and the carboxamide-linked pyrrole group of TIM1c were packed only against Tyr^{119}/Tyr^{119*}, which had a distinct orientation in comparison with TNF-TIM1 and TNF-SPD304. The phthalazine group was stabilized by a partial π-stacking interaction with Tyr^{119} and Tyr^{59} as well as hydrophobic contacts with Tyr^{59*}, Leu^{57*}, Leu^{115*}, and His^{15}. Just like SPD304, the hydrophobic ring systems of TIM1c were in close contact with the β strand (Leu^{120}-Gly^{121}-Gly^{122}) of both TNF subunits.

The molecular mechanics/Poisson-Boltzmann surface area binding affinity calculation indicated that, although the total binding free energies of TIM1 and TIM1c were less than that of SPD304, they had somewhat greater van der Waals (vdW) interaction energy (Table 3). The greater binding affinity between TNF and

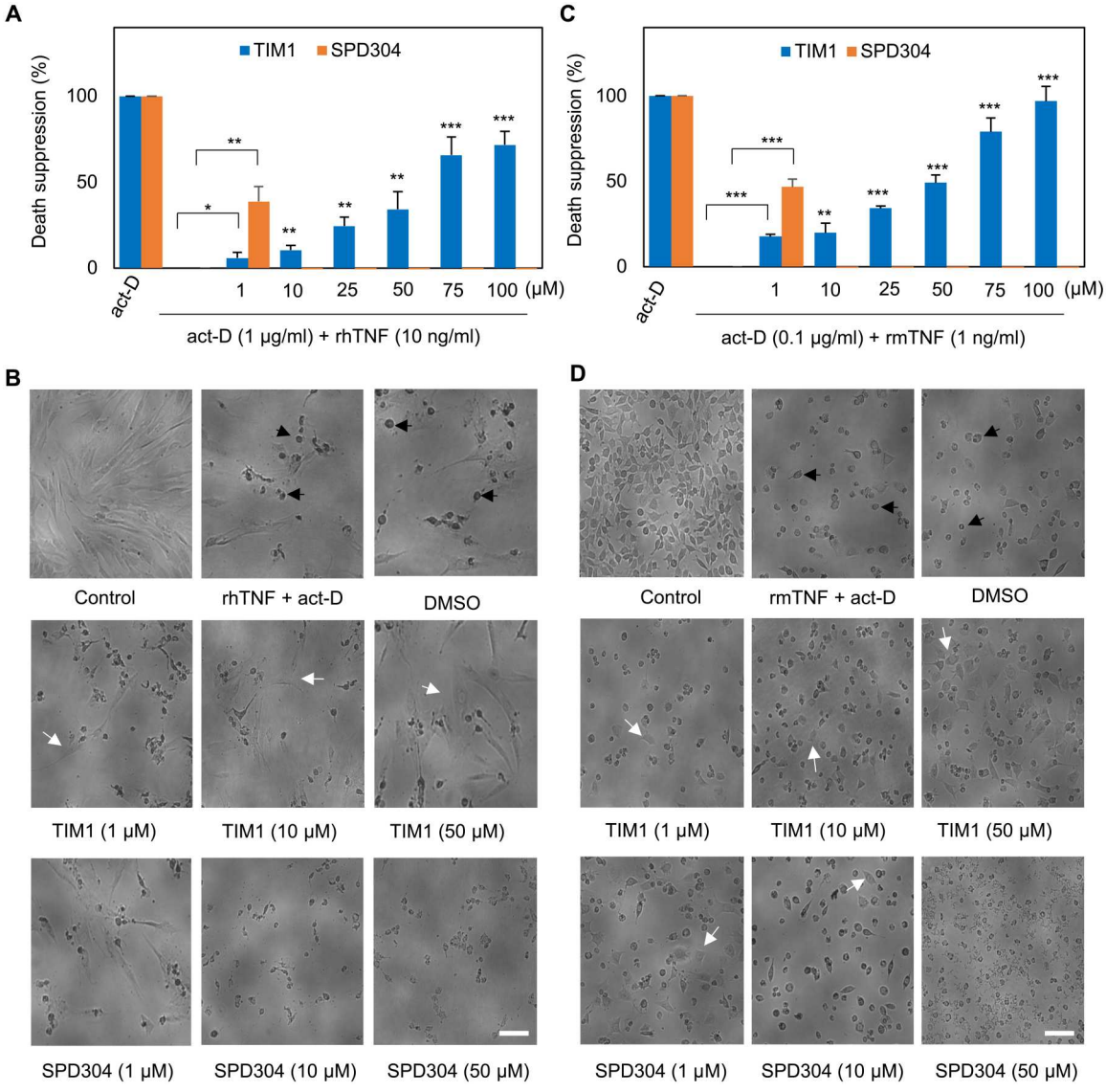

Fig. 3. The attenuation of TNF-induced cell death. (**A**) Quantification of the survival of HDFs that were treated with act-D to sensitize them to TNF-induced cell death before treatment with rhTNF and the indicated concentration of TIM1 or SPD304. $n = 4$ independent experiments. The means ± SEM of the independent experiments were subjected to two-tailed paired Student's *t* tests (*$P < 0.05$, **$P < 0.01$, and ***$P < 0.001$). (**B**) Morphology of HDFs treated as in (A). Examples of apoptotic and surviving cells are indicated with black and white arrows, respectively. Scale bar, 100 μm. (**C**) Quantification of the survival of L929 cells that were sensitized with act-D before treatment with rmTNF and the indicated concentration of TIM1 or SPD304. $n = 4$ independent experiments. The means ± SEM of the independent experiments were subjected to two-tailed paired Student's *t* tests (**$P < 0.01$ and ***$P < 0.001$). (**D**) Morphology of L929 cells treated as in (C). Examples of apoptotic and surviving cells are indicated with black and white arrows, respectively. Scale bar, 100 μm.

SPD304 was due to the higher electrostatic interaction energy of the complex, which could be attributed to the 3-trifluoromethyl group of the ligand. TIM1c had a slightly higher binding affinity than TIM1 for TNF, probably owing to the lower contribution to the polar solvation and solvent-accessible surface area energy of the complex. Given that the ligand-binding site in TNF is predominantly nonpolar, a ligand-receptor complex with greater nonpolar or vdW interaction energy is likely to favor strong binding.

TIM1c is orally bioavailable and suppresses symptoms of inflammatory arthritis in mice

Given that TIM1c potently inhibited TNF signaling in vitro, we expected that it would ameliorate RA symptoms in an animal model. The efficacy of TIM1c in the mouse model of CIA was analyzed by feeding male animals with the compound at 2 or 20 mg/kg every 2 days starting at 15 days after immunization with bovine collagen and by assessing the behavioral signs of RA up to day 60 (fig. S12). Oral administration of TIM1c caused a dose-dependent improvement in the RA symptoms of the treated groups, as indicated by a gain in body weight (Fig. 7A) and a reduction in paw volume (Fig. 7B) and squeaking number per day (Fig. 7C) in comparison

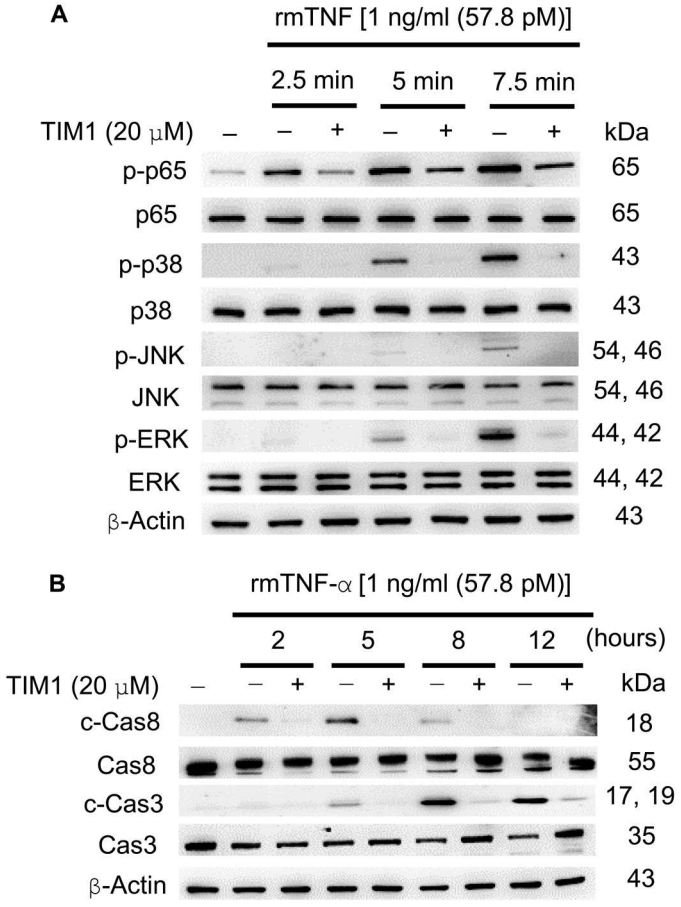

Fig. 4. Inhibition of TNF-dependent signaling pathways by TIM1. (**A**) Representative Western blot showing the activation of the NF-κB subunit p65 and the MAPKs p38, JNK, and ERK in L929 cells treated with rmTNF and TIM1 at indicated time points. β-Actin is a loading control. (**B**) Representative Western blotting for full-length (Cas8 and Cas3) and cleaved (c-Cas8 and c-Cas3) caspases in L929 cells treated with rmTNF and TIM1 at indicated time points . Blots are representative of $n = 3$ independent experiments.

with the untreated CIA group. Consequently, the arthritis index (clinical score) of the treatment groups showed a significant decline relative to the untreated CIA group (Fig. 7D). At the start of the drug treatment (day 15), the development of RA was obvious in both forelimbs and hindlimbs of CIA mice, marked by the swelling of knees, ankles, and feet (Fig. 7E). At the lower dose of 2 mg/kg per 2 days, TIM1c slightly reduced disease severity; however, at a dose of 20 mg/kg per 2 days, it substantially attenuated the induction of RA, with both forelimbs and hindlimbs appearing similar to the wild-type (no CIA) group (Fig. 7E). Hematoxylin and eosin (H&E) staining of joint tissue sections harvested at day 60 showed synovial hyperplasia, immune cell infiltration, pannus formation, thickening of synovial tissues, and narrowing of joint space in untreated CIA mice, and these phenotypes were reduced with the treatment of TIM1c in a dose-dependent manner (Fig. 7, F and G). An increase in IL-1β and IL-6 immunopositive cells was observed in the untreated CIA group, which was significantly reduced with TIM1c treatment (Fig. 7, H to J). The histological and molecular data are in agreement with the above behavioral data.

We compared the efficacy of TIM1c and TIM1 with the U.S. Food and Drug Administration–approved anti-TNF drug ETN in alleviating RA symptoms in the mouse CIA model. Male animals were given TIM1 or TIM1c (20 mg/kg; orally), or ETN (5 mg/kg; intraperitoneally) every 2 days from day 15 after the first injection of collagen until day 50. In comparison with TIM1, TIM1c showed better improvement in RA symptoms, including a gain in body weight (fig. S13A) and reductions in paw volume (fig. S13B), squeaking number (fig. S13C), and arthritis index (fig. S13D). The H&E staining of joint tissue sections showed stronger reversal of synovial hyperplasia, immune cell infiltration, pannus formation, thickening of synovial tissues, and narrowing of joint space with TIM1c as compared with TIM1 (fig. S13, E and F). TIM1c also showed a greater reduction in IL-1β and IL-6 immunopositive cells (fig. S13, G to I). The histological and molecular data are in agreement with the above-mentioned behavioral data. TIM1c showed its ability to reverse RA symptoms in CIA mice analogous to that of ETN (fig. S13, A to J). TIM1c delayed the onset of RA, but the rate of disease progression after onset was comparable to the vehicle and TNF antibody groups (fig. S13, A to D). These results suggest that TIM1c has anti-inflammatory activity and shows efficacy in mice by the oral route.

DISCUSSION

Because of the severity of diseases associated with dysregulated TNF-TNFR1 and TNF-TNFR2 signaling axes, there is a growing need to develop potent therapeutics that can prevent or suppress TNF-mediated inflammation, necroptosis, and cancerous pathways (*17*, *44*). The x-ray crystallographic structure of TNF in complex with an inhibitor, SPD304, enabled us to screen a large multiconformational library using computational drug discovery principles. We identified a new lead compound, TIM1, which inhibited TNF-induced toxicity in both human and mouse cell lines without being

Table 3. Binding free-energy (kJ mol^{-1}) decomposition of three representative TNF-ligand complexes.

System	Δ_{vdW}*	Δ_{elec}†	Δ_{ps}‡	Δ_{SASA}§	ΔG_{Total}‖
TNF-SPD304	−152.82 ± 5.85	−107.36 ± 6.32	98.6 ± 5.45	−14.78 ± 5.0	−176.37 ± 7.56
TNF-TIM1c	−164.18 ± 4.8	−22.64 ± 5.01	45.46 ± 9.12	−14.36 ± 3.98	−155.72 ± 3.65
TNF-TIM1	−203.39 ± 7.26	−25.19 ± 5.74	92.72 ± 5.42	−17.93 ± 1.2	−153.78 ± 4.48
TNF-JNJ525	−178.29 ± 6.16	−32.29 ± 5.54	89.62 ± 4.49	−15.83 ± 2.2	−136.79 ± 4.48

*Van der Waals energy. †Electrostatic energy. ‡Polar solvation energy. §Solvent-accessible surface area energy. ‖Total binding free energy.

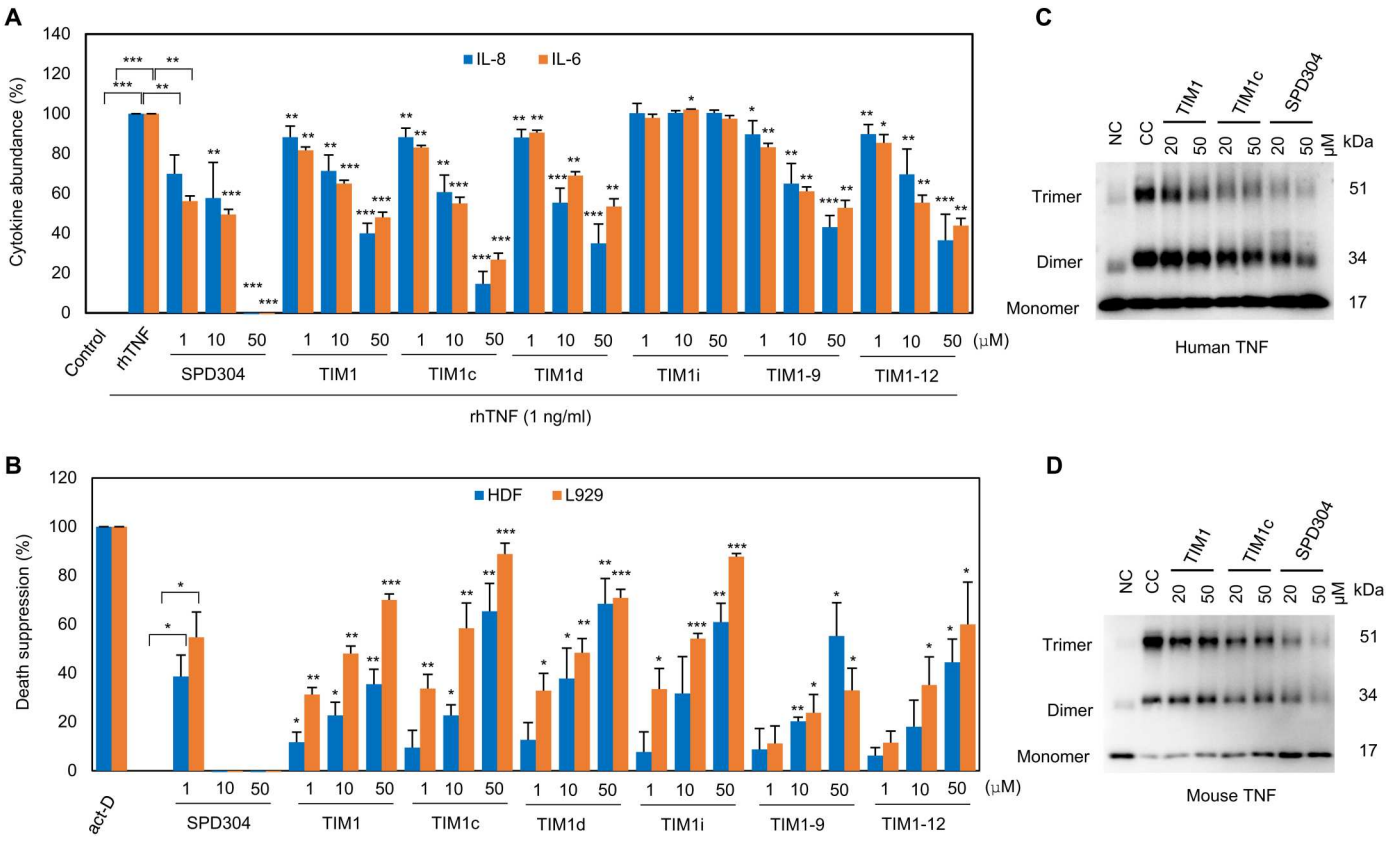

Fig. 5. In vitro activity of TIM1 derivatives and disruption of TNF homotrimerization by TIM1. (**A**) Quantification of IL-8 and IL-6 secreted by HDFs that were stimulated for 24 hours with rhTNF that had been preincubated with various concentrations of SPD304, TIM1, or the indicated TIM1 derivatives. The data were normalized to the nontreated control. $n = 5$ independent experiments. (**B**) Comparative death suppression rate (%) in HDFs and L929 cells treated with act-D to sensitize them to TNF-induced cell death before treatment with rhTNF (HDF) or rmTNF (L929) and the indicated concentration of SPD304, TIM1, or TIM1 derivatives. $n = 3$ independent experiments. The means ± SEM of the independent experiments were subjected to two-tailed paired Student's t tests (*$P < 0.05$, **$P < 0.01$, ***$P < 0.001$). (**C** and **D**) Immunoblotting for TNF in rhTNF (C) and rmTNF (D) cross-linking reactions performed in the presence of TIM1, TIM1c, or SPD304. NC, non–cross-linked control (no cross-linker, no inhibitor); CC, cross-linked control (no inhibitor). Blots are representative of three independent experiments.

toxic to the cells per se. As compared with the known inhibitor, SPD304, TIM1 demonstrated lower toxicity and marked inhibitory activity against TNF signaling. Furthermore, compound TIM1c proved to be the most potent TNF inhibitor among all TIM1 derivatives and manifested oral bioavailability in the murine CIA model to suppress various RA symptoms in the mice.

Our computational modeling suggested that TIM1 and TIM1c have a shape complementarity to the central hydrophobic cavity of the TNF dimer, with their thiazole ring stacked between Tyr^{119} from both monomers. This residue is essential for the coordination of monomer assembly and for the accommodation of SPD304 in the binding cavity of TNF (*24*). MD simulations indicated that complexes TNF-TIM1 and TNF-TIM1c were likely stabilized mostly by hydrophobic contacts without any intermolecular hydrogen bonds or salt bridges. Because the ligand-binding cavity on the TNF dimer is a rather flat surface lined predominantly by aromatic ring structures, such as tyrosine, a ligand must be hydrophobic and large enough to occupy the cavity in an extended conformation (*45*). The chemical cross-linking and Western blotting followed by the SPR spectroscopy analyses showed that TIM1 and TIM1c are specific and potent disruptors of TNF homotrimerization. Further, SPR spectroscopy demonstrated that TIM1 and TIM1c can interact directly with the TNF monomer. On the basis of this result, two probable scenarios for the mechanism of action of TIM1 or its potent derivative TIM1c can be proposed. First, the ligand may facilitate the formation of a stable homodimer by imitating the third monomer during TNF trimer assembly. Second, the ligand may bind to the homodimer only after spontaneous dissociation of one TNF molecule from the homotrimer, thereby preventing subsequent reassembly of the functional trimer. A third possible mechanism of action could be that the ligand interacts with the preformed homotrimer and displaces one of the TNF molecules from the trimeric assembly. This mechanism seems unlikely given that the ligand-binding residues of TNF monomers are buried in the protein-protein interface, requiring the inhibitor to overcome a considerable potential energy barrier to disrupt a preformed trimer (*46*).

For a few known TNF inhibitors, the definite mechanism of their inhibitory action has been determined. The inhibitors may block the cellular effect of TNF by interacting with the receptor-binding surface of TNF (*34*), by interacting with the TNF-binding surface of the receptor (*32*), by disrupting the trimerization interface of TNF (*47*), by blocking TNF-converting enzyme or other downstream signaling molecules (*48*), or by stabilizing an asymmetrical soluble

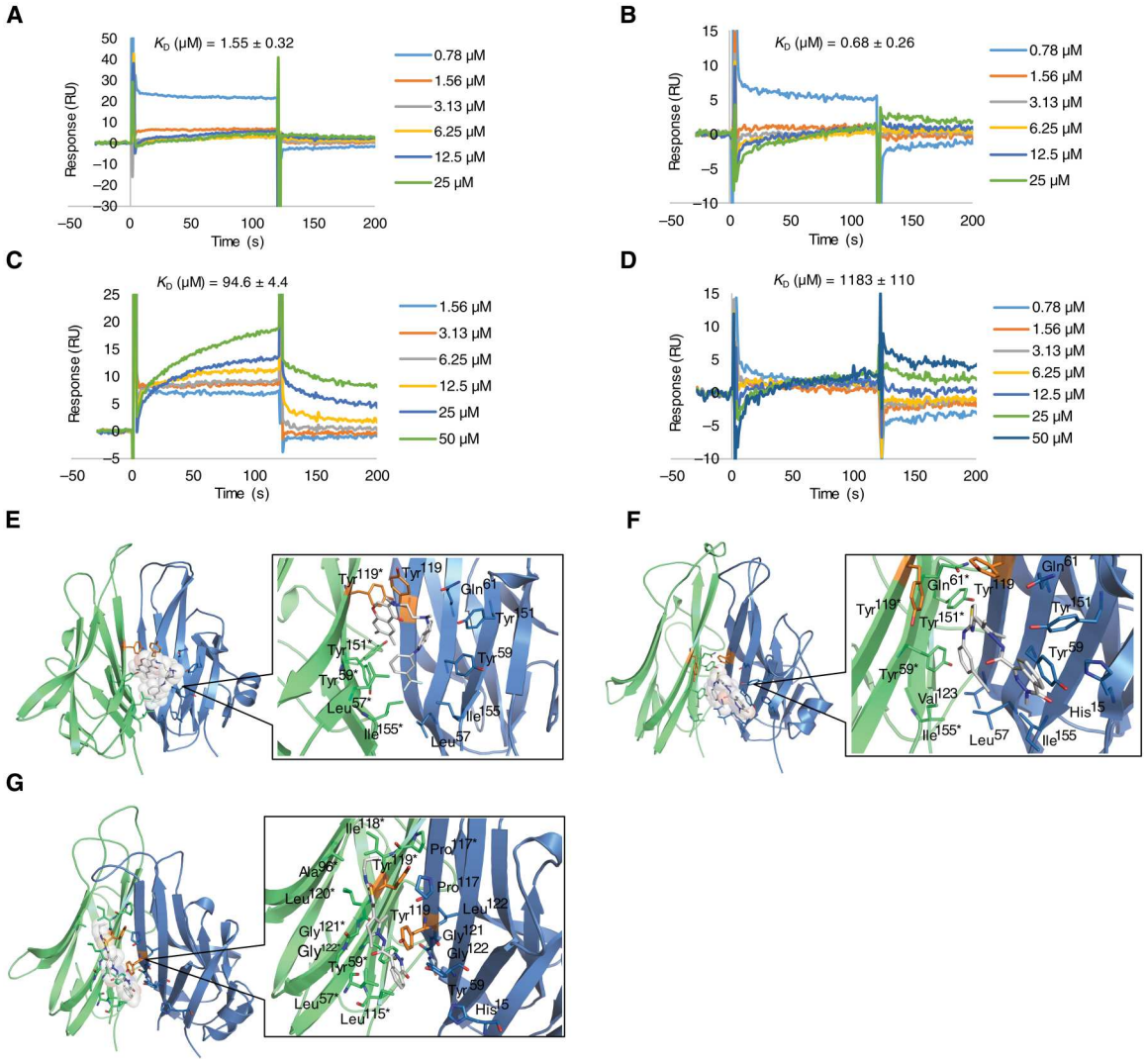

Fig. 6. Biophysical and intermolecular interaction of TIM1 and TIM1c with TNF. (**A** to **D**) SPR sensograms illustrating the biophysical interactions between TIM1 and rmTNF (A), TIM1 and rhTNF (B), TIM1c and rmTNF (C), and TIM1c and rhTNF (D). Data are the average of three independent experiments performed at various concentrations of analytes. $n = 3$ independent experiments. RU, response units. (**E** to **G**) MD simulations of the interactions of SPD304 (E), TIM1 (F), and TIM1c (G) with the ligand-binding cavity of the human TNF dimer. A magnified view is provided for a detailed illustration of the intermolecular interactions. Chain A and chain B of the TNF dimer are blue and green, respectively. The bound ligands are shown in stick models at the center of the cavity with the carbon atoms colored white. The key residues, Tyr^{119} in chain A and Tyr^{119*} in chain B, are depicted with orange sticks. An asterisk on a residue ID number indicates the B chain of the TNF dimer.

TNF trimer that has reduced signaling activity (*26*). Although all these approaches have been relatively effective in reducing TNF-induced signaling pathways, the extracellular inactivation of TNF through the disruption of its protein-protein interface seems to be the most direct and efficient way to alleviate chronic systemic inflammatory conditions. This approach is analogous to the mechanism of action of the antibodies or receptor fusion proteins, which irreversibly bind to TNF and neutralize its interaction with the receptor with high specificity (*22*).

We evaluated two TNF inhibitors, SPD304 and C87, as positive controls to compare their toxicity with TIM1 in our cell viability assay. Contrary to SPD304, C87 is reported to inhibit TNF signaling by an unknown mechanism that does not involve the disruption of the homotrimerization interface (*34*). Therefore, C87 was excluded from further activity comparison with TIM1 because the two have different mechanisms of action. We found that TIM1 has good inhibitory potency against TNF-induced cytokine secretion and inflammatory cell death without showing cytotoxicity, even at a higher concentration (up to 200 μM). The toxicity of a given ligand is normally attributed to the inherent chemical scaffolds that, after metabolic degradation, could interfere with diverse host pathways (*49*). A similarity search in chemical databases (such as PubChem) revealed that TIM1 and TIM1c do not contain any fragments that have been previously known to interact with essential host molecules, indicating their good absorption, distribution, metabolism, and excretion properties. In this regard, we observed that SPD304 has an inconsistent effect on cytokine secretion at different concentrations. For instance, the inhibition of cytokine secretion was stronger at 1 μM but weaker at 10 μM; meanwhile, SPD304 exerted a prominent cytotoxic effect at concentrations 25 to 100

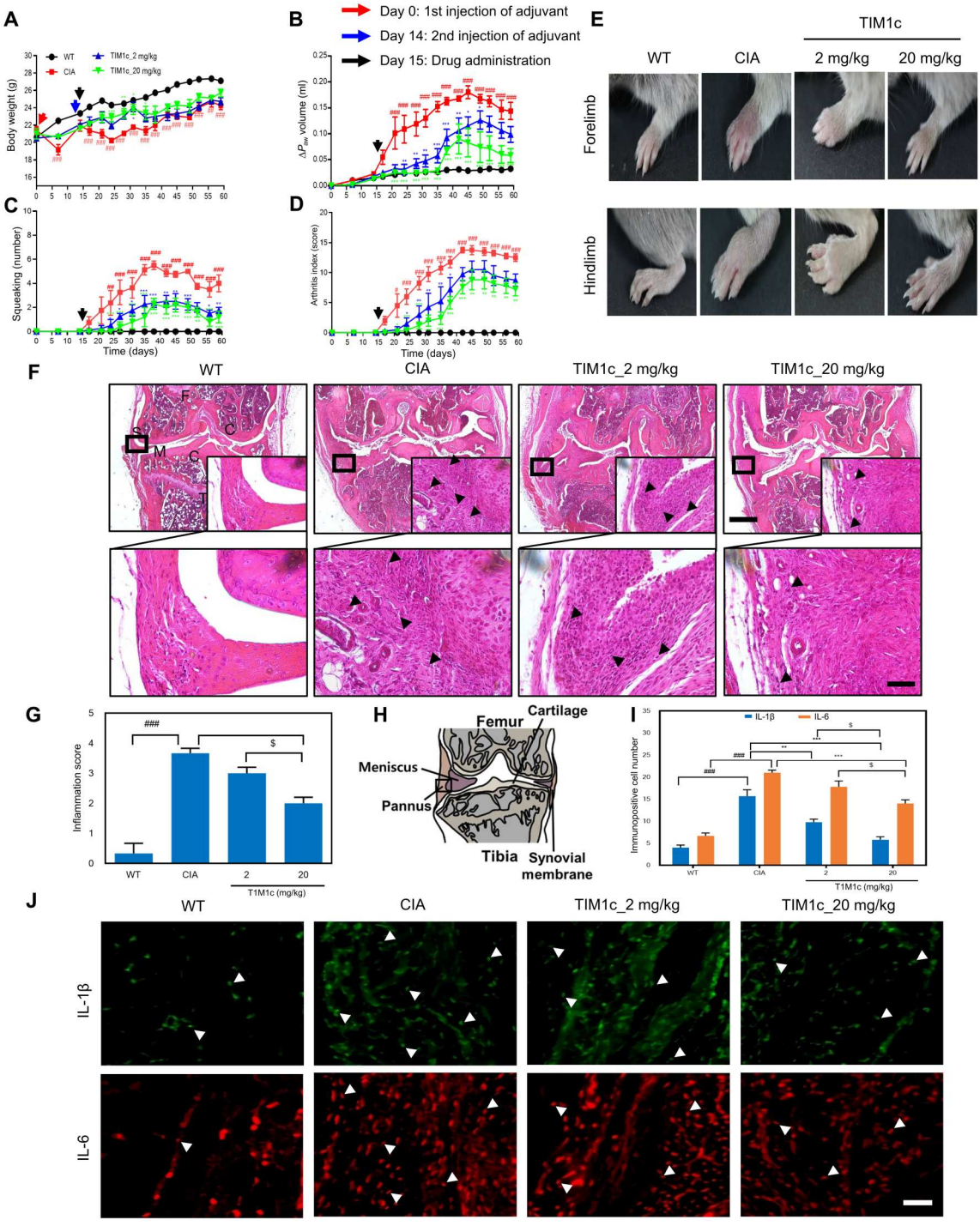

Fig. 7. Behavioral and anatomical assessment of the anti-arthritic activity of TIM1c in the CIA mouse model. (A D) EFGH J (**A** to **D**) Quantification of body weight (A), paw volume (B), squeaking score (0 represents no indication of pain) (C), and arthritis index (D) over time in CIA mice that were untreated (CIA) or treated with the indicated concentrations of TIM1 or TIM1c. Wild type (WT), no immunization to induce CIA and no drug treatment. (**E**) Representative images of limbs at the end of the experiment (day 60). (**F**) Histological images of sections through knee joints stained with hematoxylin and eosin. Scale bars, 500 μm (low magnification) and 50 μm (insets). Black arrowheads indicate immune cell infiltration. C, cartilage; S, synovial membrane; F, femur; T, tibia; M, meniscus. (**G**) The extent of inflammation was scored 0 to 4 based on the degree of swelling of the synovium, invasion of pannus, erosion of cartilage, and infiltration of immune cells; 0 = normal, 1 = slight inflammation, 2 = mild inflammation, 3 = moderate inflammation, and 4 = severe inflammation. (**H** to **J**) The black box in the cartoon (H) indicates the area of the synovial membrane and pannus in knee joint sections in which IL-1β$^+$ and IL-6$^+$ cells were quantified (I) from imaging data (J). White arrowheads in (J) indicate examples of IL-1β$^+$ and IL-6$^+$ cells. IL-1β$^+$ and IL-6$^+$ cells were counted in joint sections from at least four different mice per treatment group and averaged. Scale bar, 500 μm. All values are the means ± SEM. #P < 0.05, ##P < 0.01, and ###P < 0.001 versus the wild-type group; *P < 0.05, **P < 0.01, and ***P < 0.001 versus the CIA group; and §P < 0.05 versus TIM1c_2 mg/kg group. For all panels, n = 4 or 5 mice per treatment group.

μM. This inconsistent activity of SPD304 could be attributed to a specific chemical property that might have interfered with important cell physiological or metabolic processes. The 3-alkylindole moiety of the ligand has been proven to be metabolized by cytochrome P450, generating reactive electrophilic iminium ions that can react with key intracellular proteins and DNA (*50*). In addition, C87 exerted mild toxicity toward HDFs; in contrast, TIM1 did not yield any sign of cytotoxicity at any of the tested concentrations. Although TIM1 is somewhat less effective than SPD304 at a lower concentration (~1 μM), its safety profile is manyfold better than that of the latter from a therapeutic viewpoint (fig. S1, A and B).

We demonstrated that TIM1c has oral bioavailability and delayed the onset of RA in the murine CIA model. It is noteworthy that disease severity was attenuated with treatment at both tested doses of TIM1c. Now, only anti-TNF antibodies or decoy receptors are approved for the treatment of diseases such as RA, psoriatic arthritis, and ankylosing spondylitis (*51*). A few peptide- or peptidomimetic-based TNF inhibitors have been identified by either phage display or rational design approaches (*52*, *53*). Nevertheless, small-molecule agents are preferable to peptides or proteins because of their desirable pharmacokinetic endpoints, ensuring greater bioavailability and metabolic stability (*54*). Nevertheless, a handful of TNF-blocking small-molecule compounds have been demonstrated to be effective by oral route in animals (*55*). The efficacy of TIM1c in CIA mice suggests that the TIM series of compounds may make a valuable contribution to the existing research on the cure or prevention of TNF-mediated inflammatory diseases by means of low–molecular weight drugs.

In summary, our virtual screening workflow uncovered new small-molecule ligands with the capacity to inhibit TNF function by disrupting its homotrimerization. The oral efficacy in mice and the milder toxicity profile of the TIM series of compounds relative to existing small-molecule TNF inhibitors should encourage their future validation or improvement and characterization as valuable anti-inflammatory agents.

MATERIALS AND METHODS

Cell lines and reagents

HDFs [American Type Culture Collection (ATCC) PCS-201-012, Manassas, VA, USA] and L929 cell lines (ATCC CCL-1, NCTC clone 929) were maintained in high-glucose Dulbecco's modified Eagle's medium (Thermo Fisher Scientific Inc., catalog no. 11965092, Waltham, MA, USA) containing 0.2% of a normocin solution (InvivoGen, catalog no. ant-nr-1, San Diego, CA, USA), 1% of a HyClone penicillin/streptomycin solution (Cytiva, catalog no. SV30010, Marlborough, MA, USA), and 10% of fetal bovine serum (Thermo Fisher Scientific Inc., catalog no. 16000044). Both cell lines were incubated in a humidified atmosphere containing 5% CO_2 at 37°C (Thermo Fisher Scientific Inc.). SPD304 (MolPort ID: MolPort-042-665-817; ChemDiv, catalog no. 4031-0592), C87 (Tocris Cookson, catalog no. 5484, Bristol, UK), rmTNF (Miltenyi Biotec, catalog no. 130-101-688, Auburn, CA, USA), rhTNF (Miltenyi Biotec, catalog no. 130-094-015), act-D (Thermo Fisher Scientific Inc., catalog no. 11805017), bis(sulfosuccinimidyl)suberate (BS3; Thermo Fisher Scientific Inc., catalog no. A39266), and ETN (Sigma-Aldrich Co., catalog no. Y0001969, St. Louis, MO, USA) were purchased from the respective company mentioned in parentheses after each chemical. All test compounds were dissolved in absolute dimethyl sulfoxide (DMSO; Sigma-Aldrich Co., catalog no. D8418).

Animals

Male DBA/1J mice (20 to 23 g) were purchased from Central Lab Animal Inc. (Seoul, Korea). The animals were housed at a limited access rodent facility at a maximum of four animals per polycarbonate cage and were given free access to pelleted feed and water. The temperature was maintained at 22° to 24°C on a 12-hour light/12-hour dark cycle. The animals were acclimated for at least 1 week before the experiments. Every effort was made to minimize the number of animals used per experiment and their potential suffering. All methods were approved by the Animal Care and Use Committee of Kyung-Hee University, Korea. All procedures were executed in accordance with the Guide for the Care and Use of Laboratory Animals by the Korea National Institute of Health.

Murine CIA and experimental treatment groups

Each male DBA/1J mouse (6 weeks old) in CIA model groups was first immunized at the base of the tail by subcutaneous injection of 50 μl of an emulsion consisting of 100 μg of bovine type II collagen (Chondrex, catalog no. 20021, Woodinville, WA, USA) dissolved in 25 μl of acetic acid (Sigma-Aldrich Co., catalog no. A6283), and 25 μl of complete Freund's adjuvant (Sigma-Aldrich Co., catalog no. F5881); this time point was designated as day 0. Each mouse was then given a booster injection of 50 μl of an emulsion of the same composition except for incomplete Freund's adjuvant (Sigma-Aldrich Co., catalog no. F5506) on day 14. The experimental schedule for the establishment of the mouse model of CIA is shown in fig. S12. All the mice were subdivided randomly into various groups: the no-treatment normal group (wild type, $n = 4$ or 8), collagen-injected and vehicle-treated arthritis control group (CIA, $n = 4$ or 8), 2 mg/kg TIM1c–treated CIA group (TIM1c_2 mg/ml, $n = 4$), 20 mg/kg TIM1c–treated CIA group (TIM1c_20 mg/ml, $n = 5$ or 8), 20 mg/kg TIM1–treated CIA group (TIM1_20 mg/ml, $n = 8$), and 5 mg/kg ETN–treated CIA group (ETN_5 mg/ml, $n = 8$). TIM1 and TIM1c molecules were dissolved in 50% DMSO and fed orally to the mice. ETN was dissolved in phosphate-buffered saline (PBS) and administered intraperitoneally to the CIA mice. The treatment groups were given a dose every 2 days starting on day 15 until day 60 or 50.

Behavioral assessment of arthritis symptoms

To evaluate the progression of arthritis in the relevant groups of mice, we determined four parameters—body weight, the paw volume increase, the squeaking score, and the arthritic score—after the first immunization with collagen and complete Freund's adjuvant. The body weights of the mice were measured on a digital balance (Mettler-Toledo Inc., Columbus, OH, USA). Ankle pain was evaluated on a squeaking scale to assess nociception and hyperalgesia. Squeaking included any vocalization evoked by ankle flexion and extension. The flexion and extension procedures were repeated 10 times every 5 s, and a grade of 0 (no vocalization) or 1 (vocalization) was given for each hindlimb of a mouse. Total numbers of squeaking vocalizations detected by the observer were then calculated for the squeaking score. Paw swelling was measured by volume displacement of an electrolyte solution on a water displacement plethysmometer (Ugo-Basil Biological Research Apparatus Co., Comerio-Varese, Italy), which was described previously

(*56*). Hindlimbs were immersed to the line of hairy skin, and their volumes were read on a digital display. The paw volume increase was represented as a volume difference from day 0, which was set to 0. The arthritis index was assessed by grading apparent arthritic severity in all joints of all four limbs on a four-point scale per limb; the maximum score was 16 for each mouse, in which 0 = no erythema or swelling of any joint in one limb, 1 = erythema or swelling of at least one joint per limb, 2 = erythema or swelling of fewer than three joints per limb, 3 = erythema or swelling of all joints in one limb, and 4 = ankylosis and deformity of all joints in one limb.

Histopathological and immunohistological analyses of knee joints

The knee joints of mice groups were dissected on day 50 or 60. After removing the surrounding skin, tendon, and ligament, the solid tissues including joint bones were fixed in 10% formalin, decalcified for 3 days in CalciClear Rapid solution (National Diagnostics Co., catalog no. HS-105, Atlanta, GA), and embedded in paraffin. Coronal sections (8 μm thick) were cut through the knee joint using a manual rotary microtome (Finesse 325, Thermo Shandon Inc., Pittsburgh, PA) and stained with H&E for histological evaluation. Paraffin tissue sections obtained from mouse knees were deparaffinized in xylene (Sigma-Aldrich Co., catalog no. 95662). The tissue samples were then hydrated with ethanol (DaeJung Co., catalog no. 4023-4110, Pyeongtaek, Korea) and washed with distilled water, followed by antigen retrieval by heating with 100 mM sodium citrate tribasic dihydrate (pH 6.0; Sigma-Aldrich Co., catalog no. S4641) for 15 min using a microwave. Slides were washed with PBS for 20 min, and samples were then blocked by incubation for 2 hours in PBS with 10% goat normal serum. Primary antibodies specific for IL-1β (1:100; Santa Cruz Biotechnology, catalog no. SC7884, RRID:AB_2124476, Dallas, TX, USA) and IL-6 (1:100; Thermo Fisher Scientific Inc., catalog no. M620, RRID:AB_223576) were used. Antibodies were incubated with tissue samples overnight at 4°C in a cold chamber. After washing, the samples were incubated in the dark for 2 hours at room temperature with Alexa Fluor 568 goat anti-mouse (1:1000; Thermo Fisher Scientific Inc., catalog no.A21043, RRID:AB_2535712) and Alexa Fluor 488 goat anti-rabbit (1:1000; Thermo Fisher Scientific Inc., catalog no.A11034, RRID:AB_2576217) secondary antibodies, respectively. The section samples were washed with phosphate-buffered saline with Tween-20 (PBST) and mounted on a microslide glass with histological mounting medium (Thermo Fisher Scientific Inc., catalog no. ICN622701, RRID:AB_2334979). The samples were examined with a confocal laser scanning microscope (FV10i-w-set, Olympus Co., Japan). The numbers of immunopositive cells in each group were counted and calculated in the predefined square area including the synovial membrane and pannus (black box in Fig. 7H). The areas were arbitrarily selected within the folded synovium, which lines the inner surface of the fibrous outer capsule of the joint and its abnormal fibrovascular tissue, pannus.

Cell viability assay

A colorimetric MTT assay (Thermo Fisher Scientific Inc., catalog no. M6494) was carried out to measure cell viability. HDFs were seeded in 96-well plates (BD Biosciences, San Jose, CA, USA) at a density of 10^4 per well and grown overnight and then incubated with different concentrations of the test compounds for 24 hours. The next day, the medium was replaced with 10% of the MTT solution in the culture medium (100 μl per well) and incubated for 3 hours at 37°C. This solution was then replaced with DMSO (100 μl per well), and the plates were incubated at room temperature for 30 min. After that, the plates were read at 540-nm wavelength using a Synergy HTX Multi-Mode Microplate Reader (BioTek Instruments, Winooski, VT, USA). The LC_{50} values were determined by using an ATT Bioquest LC_{50} calculator (www.aatbio.com/tools/lc50-calculator).

IL-8 and IL-6 cytokine assays

HDFs were seeded in a 96-well plate (BD Biosciences) at the density of 10^4 per well and grown overnight. The cells were treated for 24 hours with a preincubated (for 1 hour) mixture of rhTNF and one of the test compounds. IL-8 and IL-6 secretion was assessed with the IL-8 Human Uncoated ELISA Kit (Thermo Fisher Scientific Inc., catalog no. 88-8086-88) and the IL-6 Human Uncoated ELISA Kit (Thermo Fisher Scientific Inc., catalog no. 88-7066-88), respectively. The microtiter plates were then analyzed on the Synergy HTX Multi-Mode Microplate Reader (BioTek Instruments, Winooski, VT, USA) at the appropriate wavelengths.

Cell death attenuation assays

HDFs (10^4 per well) and L929 cell lines (1.5×10^4 per well) were seeded in a 96-well plate and grown overnight under suitable conditions. The next day, the HDFs and L929 cells were pretreated with act-D (1.0 and 0.1 μg/ml, respectively) and incubated for 30 min. After that, the preincubated (for 1 hour) mixture of rhTNF (10 ng/ml) with each of the test compounds or rmTNF (1.0 ng/ml) with each of the test compounds was applied to the HDFs and L929 cells, respectively. The cells were incubated for 24 hours after treatment, and survival was measured by the MTT assay. The cell viability was calculated with reference to the no-treatment control. The obtained values were normalized to the act-D treatment group and were then used to calculate the death suppression (%) rate by the following formula

$$\text{Death suppression } (\%) = 100 - \left(\frac{100 - \text{sample value}}{100 - \text{ActD\&TNF}\alpha \text{ cotreatment value}} * 100\right)$$

The images of the treated wells were captured by means of an inverted microscope (Olympus IX53; Olympus Corporation, Tokyo, Japan).

Western blot analyses

The total protein was extracted from treated cells using the M-PER Mammalian Protein Extraction Reagent (Thermo Fisher Scientific Inc., catalog no. 78501). Briefly, cell pellets were dissolved in a mixture of M-PER and Halt Protease and Phosphatase Inhibitor Cocktail (Thermo Fisher Scientific Inc., catalog no. 78440) at 4°C for 10 min, and the obtained lysates were centrifuged for 10 min at 16,000*g* and 4°C. The supernatant, containing proteins, was collected into a separate Eppendorf tube and was subjected to the bicinchoninic acid assay (Sigma-Aldrich Co., catalog no. B9643-1 L) for protein quantification. Next, 20 μg of protein samples were loaded on a 10 to 12% SDS–polyacrylamide gel electrophoresis (SDS-PAGE), and the separated proteins were transferred to a nitrocellulose membrane (Hybond ECL; Amersham Pharmacia Biotech

Inc., Piscataway, NJ, USA) in a Mini-PROTEAN Tetra Cell and Mini Trans-Blot Electrophoretic Transfer Cell System (Bio-Rad Laboratories, Hercules, CA, USA). The membrane blocking was performed with 5% nonfat dried milk (Bio-Rad Laboratories, catalog no. 1706404) for 1 hour. The membranes were immunoblotted with specific primary antibodies such as antibodies against phospho-p65 (p65) (Cell Signaling Technology, catalog no. 3033, RRID:AB_331284), p65 (Cell Signaling Technology, catalog no. 6956, RRID:AB_10828935), p-JNK (Cell Signaling Technology, catalog no. 9251, RRID:AB_331659), JNK (Cell Signaling Technology, catalog no. 9252, RRID:AB_2250373), p-p38 (Cell Signaling Technology, catalog no. 9211, RRID:AB_331641), p38 (Cell Signaling Technology, catalog no. 9212, RRID:AB_330713), ERK (Cell Signaling Technology, catalog no. 9102, RRID:AB_330744), Cas3 (Cell Signaling Technology, catalog no. 9662, RRID:AB_331439), Cas8 (Cell Signaling Technology, catalog no. 4790, RRID:AB_10545768), p-ERK (Santa Cruz Biotechnology, catalog no. sc-81492, RRID:AB_1125801), and β-actin (Santa Cruz Biotechnology, catalog no. sc-47778, RRID:AB_626632) with gentle shaking at 4°C overnight. The next day, after rigorous washing with PBS supplemented with 0.1% Tween 20, the membranes were incubated with a peroxidase-conjugated goat anti-mouse immunoglobulin G (IgG) (Thermo Fisher Scientific Inc., catalog no. 31430, RRID:AB_228307) or goat anti-rabbit IgG (Thermo Fisher Scientific Inc., catalog no. 31460, RRID:AB_228341) antibody for 2 hours at room temperature. The proteins were treated with the SuperSignal West Pico PLUS Chemiluminescent Substrate (Thermo Fisher Scientific Inc., catalog no. 34580) and visualized on a ChemiDoc Touch Imaging System (Bio-Rad Laboratories).

Disruption of TNF trimerization assembly

Inhibitors were incubated with 100 ng of recombinant TNF at 37°C for 1 hour and were cross-linked with 4.8 mM BS3 (Thermo Fisher Scientific Inc.) for 30 min at room temperature. Next, $^{1}/_{10}$ volume of 1 M tris-HCl (pH 7.5; Thermo Fisher Scientific Inc., catalog no. 15567027) was added to stop the reaction. After that, the samples were separated by SDS-PAGE and immunoblotted for TNF (Cell Signaling Technology, catalog no. 3707, RRID:AB_2240625).

SPR spectroscopy

The biophysical interaction of TIM1 and TIM1c with rmTNF and rhTNF was determined by conducting an SPR analysis on Biacore 2000 (Cytiva, Emeryville, CA, USA). The rmTNF and rhTNF were dissolved in 5 mM sodium acetate solution (pH 4.0; XanTec bioanalytics GmbH, catalog no. B A5-40, Düsseldorf, Germany) at the concentration of 50 and 20 μg/ml for immobilization on the surface of an HC1000M sensor chip (XanTec bioanalytics GmbH, catalog no. SCB HC1000M) by an amine coupling kit (XanTec bioanalytics GmbH, catalog no. K AN-50). PBS (pH 7.4; Gibco, catalog no. 70011044) was used as a running buffer, and 10 mM glycine-HCl (pH 1.5; XanTec bioanalytics GmbH, catalog no. B G15-50) was used as a regeneration buffer. The analytes (TIM1 and TIM1c) were applied at various concentrations ranging from 0.78 to 50 μM with a flow rate of 30 μl/min. The injection of running buffer into the empty channel served as a reference. The experiments were performed three times with freshly prepared reagents, and the BIAevaluation software (BIAcore AB, Uppsala, Sweden) was used to analyze the data.

Computational methods

The screening library was constructed using chemical structures offered by ZINC (drug-like and lead-like) and different vendors (Fig. 1 and Table 1). The chemical structures were prepared by means of the sdwash tool of the Molecular Operating Environment (MOE) software (*57*). The ligand structures were cleaned by the removal of disconnected salt atoms and inorganic metal ions as well as ligands carrying reactive groups. For ligands with broken fragments, only the largest fragments were kept. Explicit hydrogen atoms were added, and the protonation states were adjusted by deprotonating strong acids by protonating strong bases. Up to 10 tautomeric states were enumerated for each ligand, and the intramolecular bonds were scaled to reasonable lengths. The cleaned structures were energy-minimized using the MMFF94x force field until a root mean square gradient of 0.1 was reached. Partial charges were calculated for the ligand atoms before the energy minimization with the MMFF94x force field.

Calculation of molecular fingerprint–based ligand similarity

Molecular fingerprints were calculated for each ligand in the database to emphasize molecular attributes according to the bit-packed MACCS Structural Keys (FP:BIT_MACCS) scheme. An in-house support vector language script was applied to identify the ligands that are at least 60 to 80% similar to a selected set of known TNF inhibitors reported in the literature. The search was performed by means of a Tanimoto similarity metric, Tanimoto coefficient, which measures the similarity between two fingerprints by the formula #AB / (#A + #B − #AB), in which A and B are the two fingerprints and # represents the number of features in each. The resultant ligands were stored in a separate library for subsequent screening.

Pharmacophore modeling

We set up pharmacophore models based on two inhibitors, JNJ525 and SPD304, and performed a ligand-based screening of ligands. A Planar-Polar-Charged-Hydrophobic scheme was used to create pharmacophore features around the essential ligand groups. Four pharmacophore features were created on each of the ligands on the basis of their observed interaction with the TNF-α residues. The resultant hits were kept in a different library for structure-based virtual screening.

Virtual screening

Two separate virtual screenings were carried out, one using the TNF/SPD304 complex (PDB ID: 2AZ5) and the other using the TNF/JNJ525 complex (PDB ID: 5MU8). The TNF-α atoms were kept rigid, whereas ligand atoms were flexible. The docking was performed with a triangle-matcher placement method and London dG scoring function, retaining up to 30 docked poses of each ligand. The top-scoring poses of each ligand were subjected to another round of the docking run with MMFF94x force field refinement and the GBVI/WSA ΔG scoring function. The GBVI/WSA ΔG is a force field–based scoring function, which estimates the free energy of binding of the ligand from a given pose. The functional form is explained by the following equation

$$\Delta G \approx c + \alpha \left[\frac{2}{3}\left(\Delta E_{\mathrm{Coul}} + \Delta E_{\mathrm{sol}}\right) + \Delta E_{\mathrm{vdW}} + \beta \Delta \mathrm{SA}_{\mathrm{weighted}}\right]$$

where c represents the average gain/loss of rotational and translational entropy; α and β are constants, which were determined during training (along with c) and are force field dependent; E_{Coul} is the coulombic electrostatic term, which is calculated using currently loaded charges using a constant dielectric of $\varepsilon_i = 1$; E_{sol} is the solvation electrostatic term, which is calculated using the GBVI solvation model; E_{vdW} is the vdW contribution to binding; and $SA_{weighted}$ is the surface area weighted by exposure. At the final step, the resultant docked conformations of ligands were screened on the basis of the electron density of the original ligand in the TNF cavity.

In silico toxicity prediction

The top 100 highest-scoring ligands from the virtual screening hit library were subjected to in silico toxicity prediction using open-source tools ProTox (*58*), TEST (U.S. Environmental Protection Agency, Washington, DC), DataWarrior (*59*), and PAINS-Remover (*60*). The top 10 ligands without any toxic fragments were purchased for the experimental validation of their anti-TNF activity.

MD simulation of complexes TNF-SPD304 and TNF-JNJ525

The crystal structures of TNF complexed with SPD304 and JNJ525 were retrieved from the PDB. Topologies of the ligands were obtained from the automated topology builder (ATB 3.0) server (*61*). Energy minimization and MD simulations were carried out with the gromos96-54a6 force field in GROningen MAchine for Chemical Simulations (GROMACS) 5.1.5 software (*62*). The protein-ligand complexes were embedded inside cubic boxes with a distance of 20 Å between their surface and the box boundary. Simple point charge (SPC216) water molecules were added to the simulation box, and an appropriate amount of counterions was added to neutralize the total charge of the simulation system. Energy minimization was performed by the steepest-descent algorithm until a maximum force of 1000 kJ mol^{-1} nm^{-1} was reached. The temperature of the simulation system was equilibrated according to the V-rescale scheme, a modified version of the Berendsen temperature-coupling scheme. Pressure equilibration was achieved by the Parrinello-Rahman algorithm at 1 bar. During the temperature and pressure equilibration processes, the backbone heavy atoms of the protein were harmonically restrained for 100 ps. The production run was carried out for 100 ns without position restraints on the backbone atoms. The periodic boundary condition was applied for the simulation system, and all bonds involving hydrogen atoms were constrained with a linear constraint solver algorithm. A timestamp of 0.002 ps was used, and trajectory snapshots were saved every 10 ps. Data analysis was performed in VMD (*63*), PyMOL (Schrödinger, LLC, New York, NY, USA), Discovery Studio 4.0 (Dassault Systèmes, Vélizy-Villacoublay, France), MOE software, and by built-in tools of the GROMACS software.

Identification of structural derivatives of TIM1

To improve the activity of TIM1, we carried out a similarity search in the MolPort database (www.molport.com/shop/index) using the TIM1 structure and specifying a Tanimoto metric cutoff of 0.8 (80% similarity cutoff). A total of 100 derivatives were selected in a spatial data file for in silico docking in MOE. The ligands were washed, and energy was minimized by the sdwash protocol of MOE. Molecular docking was performed in the SPD304 binding site of TNF (PDB ID: 2AZ5), and the docked poses were ranked on the basis of their binding affinity scores (*S* score). After rescoring with MMFF94x force field refinement and the Affinity dG scoring function, we selected the ligands showing greater affinity than did the original compound (TIM1) for experimental validation. These ligands were designated TIM1a to TIM1o. Further, another round of derivative search was carried out with a similarity cutoff ranging from 60 to 70%, and the resultant ligands were named TIM1-1 to TIM1-12.

MD simulation of the TNF-TIM1 and TNF-TIM1c complexes

A round of 100-ns MD simulation was performed on the complex of TNF-α with either TIM1 or its potent derivative, TIM1c, to analyze the intermolecular interactions under dynamic conditions. Ligand topologies were obtained from the ATB 3.0 server, and MD simulation was carried out with the parameters described in the previous section.

Construction of the free-energy landscape

The free-energy landscape (FEL) was constructed to extract the lowest-energy conformations of ligand-bound TNF to be used in the virtual screening. A cluster analysis was performed on each MD trajectory, and all conformations from the largest cluster were subjected to the calculation of the FEL. The gmx sham tool of GROMACS was used to calculate the FEL values, and the plot was generated in a demo version of the Mathematica software (version 11.2; Wolfram Research Inc., Champaign, IL, USA). A representative low-energy conformation was extracted from the FEL for docking or visual representation.

Computation of binding free energy

The binding affinities of the TNF-ligand complexes were calculated by the molecular mechanics Poisson-Boltzmann surface area calculation method. The calculation was conducted on all conformations between the 90- and 100-ns MD trajectory in the g_mmpbsa software (*64*) with Eq. 1

$$\Delta G_{bind} = \langle G_{complex} \rangle - \langle G_{protein} \rangle - \langle G_{ligand} \rangle \quad (1)$$

where G_{bind} is the total binding free energy, whereas $G_{complex}$, $G_{protein}$, and G_{ligand} are the average free energies of the complex, protein, and ligand, respectively. The free energy of each component was calculated using Eq. 2

$$G = G_{bond} + G_{ele} + G_{vdW} + G_{pol} + G_{npol} - TS \quad (2)$$

where G_{bond} is the sum of the bond, angle, and dihedral energies; G_{ele} and G_{vdW} are the electrostatic and vdW energies, respectively, derived from the calculation of the molecular mechanics energy; and G_{pol} and G_{npol} are the polar and nonpolar contributions to the solvation energy, respectively, with G_{pol} obtained by solving the Poisson-Boltzmann equation and G_{npol} estimated from its linear relationship with the solvent-accessible surface area. Configurational entropy is typically ignored because of the increased computational costs and overestimation of binding free energy values.

Statistical analysis

All in vitro data analyses were performed by two-tailed paired Student's *t* test in either Excel 2016 (Microsoft, Redmond, WA, USA) or GraphPad Prism 7 (GraphPad Software, San Diego, CA, USA).

Statistically significant differences between mouse groups were identified by two-way analysis of variance (ANOVA) followed by the Bonferroni posttest correction (for multiple comparisons of body weight, squeaking score, the paw volume increase, and arthritis index) and one-way ANOVA followed by the Tukey post hoc test (for inflammation score). P values < 0.05 were considered statistically significant. "n" represents the number of biological replicates in which each replicate experiment included two technical replicates.

Supplementary Materials

This PDF file includes:
Figs. S1 to S13
Table S1

Other Supplementary Material for this manuscript includes the following:
MDAR Reproducibility Checklist

View/request a protocol for this paper from *Bio-protocol*.

REFERENCES AND NOTES

1. B. B. Aggarwal, S. C. Gupta, J. H. Kim, Historical perspectives on tumor necrosis factor and its superfamily: 25 years later, a golden journey. *Blood* **119**, 651–665 (2012).
2. J. Vilcek, First demonstration of the role of TNF in the pathogenesis of disease. *J. Immunol.* **181**, 5–6 (2008).
3. F. C. Victor, A. B. Gottlieb, TNF-alpha and apoptosis: Implications for the pathogenesis and treatment of psoriasis. *J. Drugs Dermatol.* **1**, 264–275 (2002).
4. J. Brynskov, P. Foegh, G. Pedersen, C. Ellervik, T. Kirkegaard, A. Bingham, T. Saermark, Tumour necrosis factor alpha converting enzyme (TACE) activity in the colonic mucosa of patients with inflammatory bowel disease. *Gut* **51**, 37–43 (2002).
5. W. Swardfager, K. Lanctot, L. Rothenburg, A. Wong, J. Cappell, N. Herrmann, A meta-analysis of cytokines in Alzheimer's disease. *Biol. Psychiatry* **68**, 930–941 (2010).
6. Y. Dowlati, N. Herrmann, W. Swardfager, H. Liu, L. Sham, E. K. Reim, K. L. Lanctot, A meta-analysis of cytokines in major depression. *Biol. Psychiatry* **67**, 446–457 (2010).
7. R. M. Locksley, N. Killeen, M. J. Lenardo, The TNF and TNF receptor superfamilies: Integrating mammalian biology. *Cell* **104**, 487–501 (2001).
8. C. Monaco, J. Nanchahal, P. Taylor, M. Feldmann, Anti-TNF therapy: Past, present and future. *Int. Immunol.* **27**, 55–62 (2015).
9. R. A. Black, C. T. Rauch, C. J. Kozlosky, J. J. Peschon, J. L. Slack, M. F. Wolfson, B. J. Castner, K. L. Stocking, P. Reddy, S. Srinivasan, N. Nelson, N. Boiani, K. A. Schooley, M. Gerhart, R. Davis, J. N. Fitzner, R. S. Johnson, R. J. Paxton, C. J. March, D. P. Cerretti, A metalloproteinase disintegrin that releases tumour-necrosis factor-alpha from cells. *Nature* **385**, 729–733 (1997).
10. H. Wajant, K. Pfizenmaier, P. Scheurich, Tumor necrosis factor signaling. *Cell Death Differ.* **10**, 45–65 (2003).
11. E. Douni, G. Kollias, A critical role of the p75 tumor necrosis factor receptor (p75TNF-R) in organ inflammation independent of TNF, lymphotoxin alpha, or the p55TNF-R. *J. Exp. Med.* **188**, 1343–1352 (1998).
12. R. E. Kontermann, P. Scheurich, K. Pfizenmaier, Antagonists of TNF action: Clinical experience and new developments. *Expert Opin. Drug Discovery* **4**, 279–292 (2009).
13. G. Kollias, D. Kontoyiannis, Role of TNF/TNFR in autoimmunity: Specific TNF receptor blockade may be advantageous to anti-TNF treatments. *Cytokine Growth Factor Rev.* **13**, 315–321 (2002).
14. A. T. Ting, M. J. M. Bertrand, More to Life than NF-κB in TNFR1 Signaling. *Trends Immunol.* **37**, 535–545 (2016).
15. L. Wang, F. Du, X. Wang, TNF-α induces two distinct caspase-8 activation pathways. *Cell* **133**, 693–703 (2008).
16. A. Annibaldi, P. Meier, Checkpoints in TNF-induced cell death: Implications in inflammation and cancer. *Trends Mol. Med.* **24**, 49–65 (2018).
17. X. Chen, J. J. Oppenheim, Targeting TNFR2, an immune checkpoint stimulator and oncoprotein, is a promising treatment for cancer. *Sci. Signal.* **10**, eaal2328 (2017).
18. A. Moatti, J. L. Cohen, The TNF-α/TNFR2 pathway: Targeting a brake to release the anti-tumor immune response. *Front. Cell Dev. Biol.* **9**, 725473 (2021).
19. J. Keffer, L. Probert, H. Cazlaris, S. Georgopoulos, E. Kaslaris, D. Kioussis, G. Kollias, Transgenic mice expressing human tumour necrosis factor: A predictive genetic model of arthritis. *EMBO J.* **10**, 4025–4031 (1991).
20. M. J. Elliott, R. N. Maini, M. Feldmann, A. Long-Fox, P. Charles, P. Katsikis, F. M. Brennan, J. Walker, H. Bijl, J. Ghrayeb, J. N. Woody, Treatment of rheumatoid arthritis with chimeric monoclonal antibodies to tumor necrosis factor α. *Arthritis Rheum.* **36**, 1681–1690 (1993).
21. P. P. Sfikakis, The first decade of biologic TNF antagonists in clinical practice: Lessons learned, unresolved issues and future directions. *Curr. Dir. Autoimmun.* **11**, 180–210 (2010).
22. K. Lis, O. Kuzawinska, E. Balkowiec-Iskra, Tumor necrosis factor inhibitors - state of knowledge. *Arch. Med. Sci.* **10**, 1175–1185 (2014).
23. D. Wendling, F. Verhoeven, X. Guillot, C. Prati, Immunogenicity of TNF alpha inhibitors in rheumatology: Many questions, enough answers? *Expert Opin. Drug Saf.* **16**, 1–3 (2017).
24. M. M. He, A. S. Smith, J. D. Oslob, W. M. Flanagan, A. C. Braisted, A. Whitty, M. T. Cancilla, J. Wang, A. A. Lugovskoy, J. C. Yoburn, A. D. Fung, G. Farrington, J. K. Eldredge, E. S. Day, L. A. Cruz, T. G. Cachero, S. K. Miller, J. E. Friedman, I. C. Choong, B. C. Cunningham, Small-molecule inhibition of TNF-α. *Science* **310**, 1022–1025 (2005).
25. J. M. Blevitt, M. D. Hack, K. L. Herman, P. F. Jackson, P. J. Krawczuk, A. D. Lebsack, A. X. Liu, T. Mirzadegan, M. I. Nelen, A. N. Patrick, S. Steinbacher, M. E. Milla, K. J. Lumb, Structural basis of small-molecule aggregate induced inhibition of a protein-protein interaction. *J. Med. Chem.* **60**, 3511–3517 (2017).
26. J. O'Connell, J. Porter, B. Kroeplien, T. Norman, S. Rapecki, R. Davis, D. McMillan, T. Arakaki, A. Burgin, D. Fox Iii, T. Ceska, F. Lecomte, A. Maloney, A. Vugler, B. Carrington, B. P. Cossins, T. Bourne, A. Lawson, Small molecules that inhibit TNF signalling by stabilising an asymmetric form of the trimer. *Nat. Commun.* **10**, 5795 (2019).
27. H.-Y. Xiao, N. Li, J. J.-W. Duan, B. Jiang, Z. Lu, K. Ngu, J. Tino, L. M. Kopcho, H. Lu, J. Chen, Biologic-like in vivo efficacy with small molecule inhibitors of TNFα identified using scaffold hopping and structure-based drug design approaches. *J. Med. Chem.* **63**, 15050–15071 (2020).
28. A. Dömling, X. Li, TNF-α: The shape of small molecules to come? *Drug Discov. Today* **27**, 3–7 (2022).
29. V. Richmond, F. M. Michelini, C. A. Bueno, L. E. Alche, J. A. Ramirez, Small molecules as anti-TNF drugs. *Curr. Med. Chem.* **22**, 2920–2942 (2015).
30. X. Deng, X. Zhang, B. Tang, H. Liu, Q. Shen, Y. Liu, L. Lai, Design, synthesis, and evaluation of Dihydrobenzo[*cd*]indole-6-sulfonamide as TNF-α Inhibitors. *Front. Chem.* **6**, 98 (2018).
31. G. Melagraki, E. Ntougkos, V. Rinotas, C. Papaneophytou, G. Leonis, T. Mavromoustakos, G. Kontopidis, E. Douni, A. Afantitis, G. Kollias, Cheminformatics-aided discovery of small-molecule Protein-Protein Interaction (PPI) dual inhibitors of Tumor Necrosis Factor (TNF) and Receptor Activator of NF-κB Ligand (RANKL). *PLOS Comput. Biol.* **13**, e1005372 (2017).
32. S. Chen, Z. Feng, Y. Wang, S. Ma, Z. Hu, P. Yang, Y. Chai, X. Xie, Discovery of novel ligands for TNF-α and tnf receptor-1 through structure-based virtual screening and biological assay. *J. Chem. Inf. Model.* **57**, 1101–1111 (2017).
33. Q. Shen, J. Chen, Q. Wang, X. Deng, Y. Liu, L. Lai, Discovery of highly potent TNFα inhibitors using virtual screen. *Eur. J. Med. Chem.* **85**, 119–126 (2014).
34. L. Ma, H. Gong, H. Zhu, Q. Ji, P. Su, P. Liu, S. Cao, J. Yao, L. Jiang, M. Han, X. Ma, D. Xiong, H. R. Luo, F. Wang, J. Zhou, Y. Xu, A novel small-molecule tumor necrosis factor α inhibitor attenuates inflammation in a hepatitis mouse model. *J. Biol. Chem.* **289**, 12457–12466 (2014).
35. H. Choi, Y. Lee, H. Park, D. S. Oh, Discovery of the inhibitors of tumor necrosis factor alpha with structure-based virtual screening. *Bioorg. Med. Chem. Lett.* **20**, 6195–6198 (2010).
36. C. S. Chen, C. M. Tan, C. H. Huang, L. C. Chang, J. P. Wang, F. C. Cheng, J. W. Chern, Discovery of 3-(4-bromophenyl)-6-nitrobenzo[1.3.2]dithiazolium ylide 1,1-dioxide as a novel dual cyclooxygenase/5-lipoxygenase inhibitor that also inhibits tumor necrosis factor-alpha production. *Bioorg. Med. Chem.* **18**, 597–604 (2010).
37. Y. Cao, Y. H. Li, D. Y. Lv, X. F. Chen, L. D. Chen, Z. Y. Zhu, Y. F. Chai, J. P. Zhang, Identification of a ligand for tumor necrosis factor receptor from Chinese herbs by combination of surface plasmon resonance biosensor and UPLC-MS. *Anal. Bioanal. Chem.* **408**, 5359–5367 (2016).
38. Z. Hu, J. Qin, H. Zhang, D. Wang, Y. Hua, J. Ding, L. Shan, H. Jin, J. Zhang, W. Zhang, Japonicone A antagonizes the activity of TNF-α by directly targeting this cytokine and selectively disrupting its interaction with TNF receptor-1. *Biochem. Pharmacol.* **84**, 1482–1491 (2012).
39. S. Grootjans, T. Vanden Berghe, P. Vandenabeele, Initiation and execution mechanisms of necroptosis: An overview. *Cell Death Differ.* **24**, 1184–1195 (2017).
40. B. B. Aggarwal, Nuclear factor-κB: The enemy within. *Cancer Cell* **6**, 203–208 (2004).
41. P. Gough, I. A. Myles, Tumor necrosis factor receptors: Pleiotropic signaling complexes and their differential effects. *Front. Immunol.* **11**, 585880 (2020).
42. E. Elinav, R. Nowarski, C. A. Thaiss, B. Hu, C. Jin, R. A. Flavell, Inflammation-induced cancer: Crosstalk between tumours, immune cells and microorganisms. *Nat. Rev. Cancer* **13**, 759–771 (2013).

43. D. Brenner, H. Blaser, T. W. Mak, Regulation of tumour necrosis factor signalling: Live or let die. *Nat. Rev. Immunol.* **15**, 362–374 (2015).
44. P. Li, Y. Zheng, X. Chen, Drugs for autoimmune inflammatory diseases: From small molecule compounds to Anti-TNF biologics. *Front. Pharmacol.* **8**, 460 (2017).
45. L. Jin, W. Wang, G. Fang, Targeting protein-protein interaction by small molecules. *Annu. Rev. Pharmacol. Toxicol.* **54**, 435–456 (2014).
46. M. R. Arkin, Y. Tang, J. A. Wells, Small-molecule inhibitors of protein-protein interactions: Progressing toward the reality. *Chem. Biol.* **21**, 1102–1114 (2014).
47. D. S. Chan, H. M. Lee, F. Yang, C. M. Che, C. C. Wong, R. Abagyan, C. H. Leung, D. L. Ma, Structure-based discovery of natural-product-like TNF-α inhibitors. *Angew. Chem.* **49**, 2860–2864 (2010).
48. E. Esposito, S. Cuzzocrea, TNF-alpha as a therapeutic target in inflammatory diseases, ischemia-reperfusion injury and trauma. *Curr. Med. Chem.* **16**, 3152–3167 (2009).
49. A. F. Stepan, D. P. Walker, J. Bauman, D. A. Price, T. A. Baillie, A. S. Kalgutkar, M. D. Aleo, Structural alert/reactive metabolite concept as applied in medicinal chemistry to mitigate the risk of idiosyncratic drug toxicity: A perspective based on the critical examination of trends in the top 200 drugs marketed in the United States. *Chem. Res. Toxicol.* **24**, 1345–1410 (2011).
50. H. Sun, G. S. Yost, Metabolic activation of a novel 3-substituted indole-containing TNF-alpha inhibitor: Dehydrogenation and inactivation of CYP3A4. *Chem. Res. Toxicol.* **21**, 374–385 (2008).
51. M. C. Patra, M. Shah, S. Choi, Toll-like receptor-induced cytokines as immunotherapeutic targets in cancers and autoimmune diseases. *Semin. Cancer Biol.* **64**, 61–82 (2020).
52. A. A. Alizadeh, M. Hamzeh-Mivehroud, M. Farajzadeh, S. Dastmalchi, Identification of novel peptides against TNF-α using phage display technique and in silico modeling of their modes of binding. *Eur. J. Pharm. Sci.* **96**, 490–498 (2017).
53. S. Luzi, Y. Kondo, E. Bernard, L. K. Stadler, M. Vaysburd, G. Winter, P. Holliger, Subunit disassembly and inhibition of TNFα by a semi-synthetic bicyclic peptide. *Protein Eng. Des. Sel.* **28**, 45–52 (2015).
54. A. Mocsai, L. Kovacs, P. Gergely, What is the future of targeted therapy in rheumatology: Biologics or small molecules? *BMC Med.* **12**, 43 (2014).
55. E. Coste, I. R. Greig, P. Mollat, L. Rose, M. Gray, S. H. Ralston, R. J. Van't Hof, Identification of small molecule inhibitors of RANKL and TNF signalling as anti-inflammatory and antiresorptive agents in mice. *Ann. Rheum. Dis.* **74**, 220–226 (2015).
56. J. S. Bang, D. H. Oh, H. M. Choi, B. J. Sur, S. J. Lim, J. Y. Kim, H. I. Yang, M. C. Yoo, D. H. Hahm, K. S. Kim, Anti-inflammatory and antiarthritic effects of piperine in human interleukin 1beta-stimulated fibroblast-like synoviocytes and in rat arthritis models. *Arthritis Res. Ther.* **11**, R49 (2009).
57. Molecular Operating Environment (MOE), 2022.02 Chemical Computing Group ULC, 1010 Sherbooke St. West, Suite #910, Montreal, QC, Canada, H3A 2R7, 2022.
58. P. Banerjee, A. O. Eckert, A. K. Schrey, R. Preissner, ProTox-II: A webserver for the prediction of toxicity of chemicals. *Nucleic Acids Res.* **46**, W257–W263 (2018).
59. T. Sander, J. Freyss, M. von Korff, C. Rufener, DataWarrior: An open-source program for chemistry aware data visualization and analysis. *J. Chem. Inf. Model.* **55**, 460–473 (2015).
60. J. B. Baell, G. A. Holloway, New substructure filters for removal of pan assay interference compounds (PAINS) from screening libraries and for their exclusion in bioassays. *J. Med. Chem.* **53**, 2719–2740 (2010).
61. M. Stroet, B. Caron, K. M. Visscher, D. P. Geerke, A. K. Malde, A. E. Mark, Automated Topology Builder Version 3.0: Prediction of solvation free enthalpies in water and hexane. *J. Chem. Theory Comput.* **14**, 5834–5845 (2018).
62. M. J. Abraham, T. Murtola, R. Schulz, S. Páll, J. C. Smith, B. Hess, E. Lindahl, GROMACS: High performance molecular simulations through multi-level parallelism from laptops to supercomputers. *SoftwareX* **1-2**, 19–25 (2015).
63. W. Humphrey, A. Dalke, K. Schulten, VMD: Visual molecular dynamics. *J. Mol. Graph.* **14**, 33–38 (1996).
64. R. Kumari, R. Kumar, C. Open Source, *g_mmpbsa*—A GROMACS tool for high-throughput MM-PBSA calculations. *J. Chem. Inf. Model.* **54**, 1951–1962 (2014).
65. L. Ganesan, E. Margolles-Clark, Y. Song, P. Buchwald, The food colorant erythrosine is a promiscuous protein-protein interaction inhibitor. *Biochem. Pharmacol.* **81**, 810–818 (2011).

Acknowledgments: We thank the Ministry of Science and ICT; the Ministry of Trade, Industry, and Energy, Ministry of Health and Welfare; and the National Research Foundation of Korea for supporting this study. **Funding:** This research was supported by the Korea Drug Development Fund, funded by the Ministry of Science and ICT; the Ministry of Trade, Industry, and Energy; and the Ministry of Health and Welfare (HN21C1058). This work was also supported by the National Research Foundation of Korea (2022M3A9G1014520, 2019M3D1A1078940, and 2019R1A6A1A11051471). **Author contributions:** Conceptualization: N.J., M.C.P., M.B., and S.C. Methodology and investigation: N.J., M.C.P., D.-E.C., M.B., Y.K., and G.M.C. Visualization: N.J., M.C.P., and D.C. Funding acquisition: M.S.K. and S.C. Project administration: M.S.K., D.-H.H., and S.C. Supervision: S.C. Writing—original draft: N.J., M.C.P., and D.C. Writing—review and editing: M.S.K., D.H., and S.C. **Competing interests:** The authors declare that they have no competing interests. **Data and materials availability:** All data needed to evaluate the conclusions in the paper are present in the paper or the Supplementary Materials.

Submitted 6 April 2021
Resubmitted 19 October 2021
Accepted 13 October 2022
Published 8 November 2022
10.1126/scisignal.abi8713

Science Signaling

An orally active, small-molecule TNF inhibitor that disrupts the homotrimerization interface improves inflammatory arthritis in mice

Nasir JavaidMahesh Chandra PatraDa-Eun ChoMaria BatoolYoongeun KimGwang Muk ChoiMoon Suk KimDae-Hyun HahmSangdun Choi

Sci. Signal., 15 (759), eabi8713. • DOI: 10.1126/scisignal.abi8713

An oral route to TNF inhibition

Excessive production of the proinflammatory cytokine TNF drives many inflammatory diseases. Current targeted therapies for these conditions consist mainly of costly biologics that must be injected. Existing small-molecule inhibitors of TNF are either highly toxic or have low potency, limiting their usefulness as drugs. Javaid *et al.* identified a nontoxic TNF-inhibiting compound that they called TIM1 and that inhibited TNF signaling in mouse and human cells by disrupting TNF homotrimerization. Oral delivery of TIM1 or a more potent derivative, TIM1c, improved symptoms and delayed disease progression in a mouse model of inflammatory arthritis to a similar extent as injection of the FDA-approved TNF-targeting biologic etanercept. This compound may be a promising lead compound for future drug development efforts and a useful research tool as an alternative to more toxic TNF-inhibiting compounds.